Monthly Notices
of the
ROYAL ASTRONOMICAL SOCIETY

MNRAS **449,** 506–527 (2015) doi:10.1093/mnras/stv271

The branchings of the main *s*-process: their sensitivity to α-induced reactions on ^{13}C and ^{22}Ne and to the uncertainties of the nuclear network

S. Bisterzo,[1,2]★ R. Gallino,[1] F. Käppeler,[3] M. Wiescher,[4] G. Imbriani,[5] O. Straniero,[6]
S. Cristallo,[6,7] J. Görres[4] and R. J. deBoer[4]

[1] *Dipartimento di Fisica, Università di Torino, via P. Giuria 1, I-10125 Torino, Italy*
[2] *INAF - Astrophysical Observatory Turin, I-10025 Pino Torinese, Turin, Italy*
[3] *Karlsruhe Institute of Technology, Campus Nord, Institut für Kernphysik, D-76021 Karlsruhe, Germany*
[4] *Joint Institute for Nuclear Astrophysics (JINA), Department of Physics, University of Notre Dame, IN 46556, USA*
[5] *Dipartimento di Scienze Fisiche, Università di Napoli Federico II, I-80138 Napoli, Italy*
[6] *INAF - Osservatorio Astronomico di Collurania, 64100 Teramo, Italy*
[7] *INFN Sezione Napoli, I-80138 Napoli, Italy*

Accepted 2015 February 9. Received 2015 January 14; in original form 2014 September 23

ABSTRACT

This paper provides a detailed analysis of the main component of the *slow* neutron capture process (the *s*-process), which accounts for the solar abundances of half of the nuclei with $90 \lesssim A \lesssim 208$. We examine the impact of the uncertainties of the two neutron sources operating in low-mass asymptotic giant branch (AGB) stars: the ^{13}C(α, n)^{16}O reaction, which releases neutrons radiatively during interpulse periods ($kT \sim 8$ keV), and the ^{22}Ne(α, n)^{25}Mg reaction, partially activated during the convective thermal pulses (TPs). We focus our attention on the branching points that mainly influence the abundance of *s*-only isotopes. In our AGB models, the ^{13}C is fully consumed radiatively during interpulse. In this case, we find that the present uncertainty associated with the ^{13}C(α, n)^{16}O reaction has marginal effects on *s*-only nuclei. On the other hand, a reduction of this rate may increase the amount of residual (or unburned) ^{13}C at the end of the interpulse: in this condition, the residual ^{13}C is burned at higher temperature in the convective zone powered by the following TP. The neutron burst produced by the ^{22}Ne(α, n)^{25}Mg reaction has major effects on the branches along the *s*-path. The contributions of *s*-only isotopes with $90 \lesssim A \leq 204$ are reproduced within solar and nuclear uncertainties, even if the ^{22}Ne(α, n)^{25}Mg rate is varied by a factor of 2. Improved β-decay and neutron capture rates of a few key radioactive nuclides would help to attain a comprehensive understanding of the solar main component.

Key words: nuclear reactions, nucleosynthesis, abundances – stars: abundances – stars: AGB and post-AGB – stars: low-mass.

1 INTRODUCTION

The classical analysis of the *s*-process (the *slow* neutron capture process) has provided a first phenomenological approach to interpret the solar *s*-distribution by means of analytical tools (Clayton & Ward 1974; Käppeler, Beer & Wisshak 1989), but it was soon clear that the solar *s*-process requires a multiplicity of neutron exposures, intuitively associated with different astrophysical sites.

The existence of the *main* component of the *s*-process was advanced by the classical analysis to reproduce the solar abundances of *s*-isotopes between $90 < A \leq 204$. Low-mass asymptotic giant branch (AGB) stars ($M \lesssim 3\,\mathrm{M}_{\odot}$) were recognized to be a most promising site for the main component (Ulrich 1973; Iben & Renzini 1983). The contribution of two additional *s*-process components was required to reproduce the solar *s*-process distribution, the so-called *weak* and *strong* components. The weak component is partly responsible for the nucleosynthesis of *s*-nuclei with $A \lesssim 90$ during the hydrostatic evolutionary phases of massive stars (Arnett & Thielemann 1999; Limongi, Straniero & Chieffi 2000; Rauscher et al. 2002). The strong component was postulated by Clayton & Rassbach (1967) to explain about half of solar ^{208}Pb, despite the astrophysical site was not identified. Successively, the strong component found a natural explanation in AGB stars with low metallicity ([Fe/H] $\lesssim -1$) and low initial mass (Gallino et al. 1998; Travaglio et al. 2001).

This paper is focused on the study of the main component.

Compared to the classical analysis, the development of the first AGB stellar models has provided a more adequate description of the dynamic environment in which the main component takes place. The

---

★ E-mail: bisterzo@ph.unito.it

Published by Oxford University Press on behalf of the Royal Astronomical Society

s-process nucleosynthesis in AGB stars occurs during the late stages of the stellar evolution, when the star has a degenerate C–O core, a thin radiative layer (He-intershell) and an expanded convective envelope. During the AGB phase, the star experiences a series of He-shell flashes called thermal pulses (TPs) triggered by the sudden activation of the 3α process at the base of the He-intershell. In such a region, free neutrons are released by two key reactions, ^{13}C(α, n)^{16}O and ^{22}Ne(α, n)^{25}Mg.

The ^{13}C(α, n)^{16}O reaction is the main neutron source in low-mass AGB stars. The ^{13}C forms in a thin zone (the ^{13}C pocket) via proton captures on the abundant ^{12}C (^{12}C(p, γ)^{13}N($\beta^+\nu$)^{13}C). The most favourable conditions for the formation of the ^{13}C pocket occur during the period immediately following a third dredge-up (TDU) episode. During a TDU, the H-burning shell is switched off and, thus, the convective envelope can penetrate inwards and carry to the surface the heavy elements previously synthesized in the He-intershell. The mechanism triggering the formation of the ^{13}C pocket is far from being understood: extant models assume that a partial amount of protons may be diffused from the convective envelope into the He- and C-rich radiative He-intershell (see discussion by Straniero, Gallino & Cristallo 2006), otherwise ^{13}C would be further converted to ^{14}N via proton captures, mainly acting as a neutron poison of the *s*-process via the ^{14}N(n, p)^{14}C reaction. Different mechanisms proposed to explain the formation of the ^{13}C pocket are objects of study.[1] When the temperature becomes larger than 0.8 × 10^8 K ($kT \sim 8$ keV, which corresponds to $T_8 \sim 0.9$), ^{13}C(α, n)^{16}O burns radiatively for an extended time-scale (some 10^4 yr), releasing a neutron density $N_{\rm n} \sim 10^7$ cm^{-3} with a large neutron exposure[2] (Straniero et al. 1995).

The second neutron source, the ^{22}Ne(α, n)^{25}Mg reaction, is partially activated at the bottom of the convective shells generated by the TPs. Starting from the large amount of ^{14}N left in the H-burning shell ashes, ^{22}Ne is produced via the ^{14}N(α, γ)^{18}F($\beta^+\nu$)^{18}O(α, γ)^{22}Ne nuclear chain. At a temperature of $T_8 = 2.5$–3 ($kT \sim 23$ keV corresponds to $T_8 \sim 2.7$), the ^{22}Ne(α, n)^{25}Mg reaction starts releasing neutrons, giving rise to a small neutron exposure with a high peak neutron density ($N_{\rm n}$(peak) $\sim 10^{10}$ cm^{-3}). Although this second burst accounts only for a few per cent of the total neutron exposure, it regulates the final abundances of the *s*-only isotopes nearby to important branch points of the *s*-process.

Arlandini et al. (1999) provided a first interpretation of the solar main component by adopting an average between two AGB stellar models with initial masses of 1.5 and 3 M$_\odot$, half-solar metallicity, and a specific ^{13}C-pocket choice (called *case ST*). The case ST was calibrated by Gallino et al. (1998) in order to reproduce the solar abundances of *s*-only isotopes between $96 \le A \le 204$ with half-solar metallicity models. The two 1.5 and 3 M$_\odot$ models were chosen as they represent the stellar mass range that better reproduces the observations of peculiar *s*-rich disc stars (Busso et al. 1995).

The complex dependence of the *s*-process on the initial chemical composition of the star was investigated by Gallino et al. (1998). They found that the strong component derives from AGB stars of low metallicity. Indeed, for any ^{13}C-pocket strength, the number of free neutrons per iron seed increases with the ^{13}C/^{56}Fe ratio, and the neutron fluence progressively overcomes the first two *s*-peaks at neutron magic numbers $N = 50$ and 82, directly feeding ^{208}Pb (explaining the previously introduced strong component).

The heterogeneity of the *s*-process is also evidenced by spectroscopic observations in different stellar populations: the discovery of the first three lead-rich low-metallicity stars confirms that ^{208}Pb may be strongly produced in peculiar objects of the Galactic halo (Van Eck et al. 2001). Moreover, the *s*-elements observed in peculiar *s*-rich stars (e.g. MS, S, C, Ba and Post-AGB stars, planetary nebulae and lead-rich stars, later called CEMP-s stars) show a scatter at a given metallicity. This scatter has been recognized since the first studies by Smith & Lambert (1990), Busso et al. (2001) and Abia et al. (2002, for recent analysis see the review by Sneden, Cowan & Gallino 2008; Käppeler et al. 2011; Karakas & Lattanzio 2014, and references therein).

At present, stellar models are not able to reproduce the observed scatter without employing a free parametrization in modelling the formation of the ^{13}C-pocket (Herwig et al. 1997, 2003; Karakas & Lattanzio 2007; Cristallo et al. 2009; Piersanti et al. 2013). Most uncertainties of stellar models are indeed related to the treatment of convective/radiative interfaces (Iben & Renzini 1983; Frost & Lattanzio 1996), which influence the extension and the ^{13}C profile of pocket, as well as the occurrence and deepness of the TDU.

Another key uncertainty of AGB stellar models results from the unknown efficiency of the mass-loss rate, which regulates the number of TPs and the AGB lifetime. This is particularly challenging in intermediate-mass AGB (Ventura & D'Antona 2005; Ventura & Marigo 2010). Despite the solar *s*-distribution between $90 < A \le 204$ receives a dominant contribution by low-mass AGB models of disc metallicity, intermediate-mass or low-metallicity AGB models are crucial to study the chemical evolution of dwarf galaxies and globular clusters showing a clear *s*-process signature (Tolstoy, Hill & Tosi 2009; Straniero, Cristallo & Piersanti 2014, and references therein), or the spectroscopic observation of peculiar Galactic stars (e.g. Rb-rich stars; Karakas, García-Hernández & Lugaro 2012; van Raai et al. 2012; low-metallicity *s*-enhanced stars as e.g. CH, CEMP-s, post-AGB stars; Bisterzo et al. 2011; Lugaro et al. 2012; De Smedt et al. 2014).

Besides the aforementioned uncertainties, nuclear and solar abundance uncertainties affect the *s*-process. Their impact may be substantially reduced by using the unbranched *s*-only ^{150}Sm as a reference isotope of the *s*-distribution (because it has well-known solar abundance and accurately determined neutron capture cross-sections of nearby nuclei; see Arlandini et al. 1999).

The *s*-process abundances observed in the Sun are the result of the complex Galactic chemical evolution (GCE), which accounts of the contribution of different stellar generations, with various masses, metallicities and *s*-process strengths. A GCE model is therefore needed to interpret the dynamics of the *s*-process over the Galactic history up to the present epoch (see e.g. Travaglio et al. 2004; Romano et al. 2010; Nomoto, Kobayashi & Tominaga 2013, and references therein).

Travaglio et al. (2004) have shown that in the GCE context low-mass AGB stars in the range of 1.5–3 M$_\odot$ provide the dominant contribution to the Solar system main and strong components.

The impact of intermediate AGB stars (IMS; $M^{\rm AGB}_{\rm ini} \sim 4$–8 M$_\odot$) on solar abundances is marginal, with the exception of a few neutron-rich isotopes (^{86}Kr and ^{87}Rb due to the branches at ^{85}Kr and ^{86}Rb; ^{96}Zr affected by the branch at ^{95}Zr; see also Bisterzo et al.

---

[1] See e.g. the opacity-induced overshooting at the base of the convective envelope obtained by Cristallo et al. (2009) by introducing in the model an exponentially decaying profile of the convective velocity. Other models investigate the effects of diffusive overshooting, rotation, magnetic fields or gravity waves (Herwig et al. 1997; Langer et al. 1999; Denissenkov & Tout 2003; Herwig, Langer & Lugaro 2003; Siess, Goriely & Langer 2004; Busso et al. 2012; Piersanti, Cristallo & Straniero 2013, see also Maiorca et al. 2012 for results in young open clusters).

[2] The neutron exposure τ is the time-integrated neutron flux, $\tau = \int N_{\rm n} v_{\rm th}\, {\rm d}t$, where $N_{\rm n}$ is the neutron density and $v_{\rm th}$ the thermal velocity.

2014). Indeed, the He-shell of IMS reaches higher temperatures than low-mass AGB stars, and the ^{22}Ne(α, n)^{25}Mg reaction is efficiently activated, producing higher peak neutron densities ($T_8 \sim 3.6$–3.7; $N_{\rm n} \sim 10^{11-13}$ cm^{-3}). Under these conditions, the ^{22}Ne(α, n)^{25}Mg reaction becomes the major neutron source (Truran & Iben 1977; Karakas et al. 2006; Karakas, García-Hernández & Lugaro 2012; Longland, Iliadis & Karakas 2012; van Raai et al. 2012; D'Orazi et al. 2013; Doherty et al. 2014; Straniero et al. 2014). Otherwise, in the more massive AGB models, the formation of the ^{13}C pocket and the occurrence of efficient TDUs may be inhibited by hot bottom burning and hot TDU events (Karakas & Lattanzio 2003; Goriely & Siess 2004; Herwig 2004). This significantly reduces the overall IMS contribution to the solar *s*-distribution.

GCE *s*-predictions yield a plausible agreement with the solar abundances of the *s*-only isotopes between ^{134,136}Ba and ^{208}Pb. The solar distribution between $90 \le A < 140$ is instead underestimated by our GCE model: an additional (unknown) 20–30 per cent contribution is required (Travaglio et al. 2004). The light element primary process postulated for this contribution is different from the *s*-process in AGB stars and from the weak *s*-process component occurring in massive stars. Its origin is largely debated in literature (see e.g. Frischknecht, Hirschi & Thielemann 2012; Pignatari et al. 2013b for a primary *s*-component in massive stars, Arcones & Thielemann 2013; Hansen, Andersen & Christlieb 2014 for *νp* process or *weak r*-process induced by explosive stellar nucleosynthesis).

For an exhaustive discussion about the *s*-process nucleosynthesis, we refer to the reviews by Wallerstein et al. (1997), Busso, Gallino & Wasserburg (1999), Herwig (2005), Straniero et al. (2006), Käppeler et al. (2011) and Karakas & Lattanzio (2014).

It is evident from the above considerations that the main-component approach does not provide a realistic interpretation of the whole solar *s*-abundances, because it does not account of all complex aspects of the *s*-process over the Galactic evolution.

Nevertheless, it is noteworthy that the solar *s*-contributions predicted by main component and GCE model are comparable in the atomic mass region between $140 \le A \le 204$ (see Bisterzo et al. 2011, 2014). Moreover, despite the remarkable discrepancy estimated by GCE and main component between $90 \lesssim A < 140$, fairly similar *s*-contributions are derived by looking at the relative isotopic predictions of a given element. The only exceptions are the rarest neutron-rich isotopes (^{86}Kr, ^{87}Rb, ^{96}Zr), which may be significantly produced in intermediate-mass AGB stars.

Therefore, the study of the main component can be considered a useful tool to investigate the nuclear aspects and the sensitivity of the solar *s*-predictions between $90 \le A \le 204$, focusing on *s*-isotopes close to the major branches of the *s*-path.

The main goal of this paper is to analyse how the uncertainties of the α-induced reactions on ^{13}C and ^{22}Ne may affect the main component.

Both ^{13}C(α, n)^{16}O and ^{22}Ne(α, n)^{25}Mg reaction rates may be affected by contributions of sub-threshold states and resonances, making the extrapolation of the laboratory cross-section measurements down to the energy range of stellar burning a complex task (Wiescher, Käppeler & Langanke 2012).

The ^{13}C(α, n)^{16}O rate may be influenced by the unknown contribution of the sub-threshold resonance at 6.356 MeV (owing to the $J^{\pi} = 1/2^{+}$ state in ^{17}O). Up to a factor of 3 uncertainty was evaluated by Angulo et al. (1999). Over the years, several analyses have been dedicated to this neutron source (Drotleff et al. 1993; Denker et al. 1995; Hale 1997; Keeley, Kemper & Khoa 2003; Kubono et al. 2003; Johnson et al. 2006; Pellegriti et al. 2008). Recent investigations have significantly improved the accuracy (down to ∼20–30 per cent; Heil et al. 2008b; Guo et al. 2012). Lately, the above resonance has been detected by La Cognata et al. (2013) with the Trojan horse method.

The ^{22}Ne(α, n)^{25}Mg rate is dominated by the well-studied resonance at 832 keV. The ^{22}Ne(α, n)^{25}Mg uncertainty at $T_8 = 3$ is mainly due to the unknown influence of a resonance at 633 keV. The large upper limit estimated by Angulo et al. (1999, up to a factor of 50) has been reduced by more than a factor of 10 with the experimental measurement by Jaeger et al. (2001). Remarkable experimental and theoretical works were carried out by Käppeler et al. (1994), Koehler (2002), Karakas et al. (2006), Ugalde et al. (2007) and Longland et al. (2012).

The study of the main component is useful to investigate the effects of the major nuclear network uncertainties on AGB *s*-predictions, especially close to the branch points.

A branch in the *s*-path occurs when neutron captures compete with β decays at unstable isotopes with half-lives of a few weeks to a few years, so that the *s*-path branches partly by β decays following the usual path in the stability valley and partly by neutron captures feeding the neutron-rich isotopes. The strength of the branching is described by the branching factor $f_\beta = \lambda_\beta/(\lambda_\beta+\lambda_{\rm n})$, where $\lambda_\beta = 1/\tau = \ln 2/t_{1/2}$ is the β-decay rate corresponding to the half-life $t_{1/2}$ (or to the mean lifetime τ). The decay pattern may include the β^-, β^+ and electron capture channels. The neutron capture rate $\lambda_{\rm n} = N_{\rm n}\langle\sigma v\rangle = N_{\rm n} v_{\rm T}\langle\sigma\rangle$ is given by the neutron density $N_{\rm n}$, the mean thermal velocity $v_{\rm T}$, the relative velocity between neutron and target v and the Maxwellian-averaged cross-section (MACS) defined as $\langle\sigma\rangle = \langle\sigma v\rangle/v_{\rm T}$. The neutron capture strength of the branching point is defined as $f_{\rm n} = \lambda_{\rm n}/(\lambda_\beta+\lambda_{\rm n})$.

The uncertainties in the experimental (n, γ) rates have been highly reduced in recent years reaching in some cases a precision smaller than 1 or 2 per cent (see e.g. Käppeler et al. 2011). However, the high *s*-process temperatures allow the low-lying excited states to be populated by the intense and energetic thermal photon bath. Because only the ground state is accessible by experiment, the effect of neutron captures in excited states has to be evaluated theoretically and suffers from large uncertainties (Rauscher & Thielemann 2000; Rauscher 2012; Reifarth, Lederer & Käppeler 2014). Even major uncertainties are associated with unstable nuclei for which no experimental measurement is available at the present time.

In addition, the β-decay rates of some radioactive isotopes may be largely affected by variations of temperature and electron density. Although the laboratory β-decay rates are accurately known (Cyburt et al. 2010), the contribution of thermally populated excited levels and the effects of unknown transitions in a strongly ionized plasma can largely modify the β-decay rates at stellar temperatures. Takahashi & Yokoi (1987) investigated the β-decay rates of unstable heavy isotopes at temperatures and electron densities typical of stellar interiors ($5 \times 10^7 \le T \le 5 \times 10^8$ K; $10^{26} \le n_{\rm e} \le 3 \times 10^{27}$ cm^{-3}), finding large deviations from the terrestrial values. The temperature dependence of branchings is even more complex, if they have isomeric states that are thermalized at high temperatures through transitions via mediating states at higher excitation energy. Consequently, the abundances of the affected *s*-only isotopes carry direct information on the physical conditions occurring during the *s*-process, i.e. neutron density, temperature and density (Käppeler et al. 1989).

In this context, the branch point isotopes ^{151}Sm, ^{163}Dy, ^{179}Hf, ^{176}Lu are remarkable examples. The β^--decay rate of ^{151}Sm increases strongly at He-shell flash temperature and regulates the abundances of the pair ^{152,154}Gd (Marrone et al. 2006; Wisshak et al. 2006a). ^{163}Dy and ^{179}Hf are terrestrially stable, but start to decay at temperatures typical of TPs producing a non-negligible *s*-process contribution to ^{164}Er and ^{180}Ta$^{\rm m}$, both usually bypassed by the *s*-path (Jaag & Käppeler 1996; Wisshak et al. 2001, 2004). Because of its long half-life, ^{176}Lu was long considered as a cosmochronometer until the decay rate was found to exhibit a very strong temperature dependence (Klay et al. 1991; Heil et al. 2008c; Mohr et al. 2009).

The β-decay rates calculated in stellar environments are subject to nuclear uncertainties difficult to estimate. Goriely (1999) recomputed the calculations of Takahashi & Yokoi (1987) by assuming a typical uncertainty of $\Delta\log ft = \pm 0.5$ for the decay rates of unknown transitions and showed that the final stellar rates may vary by up to a factor of 3 at typical *s*-process conditions (T_8 = 3 and $n_{\rm e} = 10^{27}$ cm^{-3}). Recently, the nuclear NETwork GENerator (NETGEN; Xu et al. 2013a) extrapolated the β-decay rates by Takahashi & Yokoi (1987) and their uncertainties (Goriely 1999) to an extended range of temperature and electron density. In a few cases, the β-decay properties of excited states have been measured in laboratory experiments, e.g. for long-lived isomeric states (^{180}Ta$^{\rm m}$ determined by Belič et al. 2002; or the key branch for the weak *s*-process in massive stars ^{79}Se$^{\rm m}$ studied by Klay & Käppeler 1988) or for isotopes with small *Q*-values, which are sensitive to the bound-state β-decay mechanism (examples are ^{163}Dy and ^{187}Re studied by Jung et al. 1992 and by Bosch et al. 1996, respectively). In general, however, measurements of such data remain a big experimental challenge (Reifarth et al. 2014).

The paper is organized as follows. We start with a description of the solar main component, updated with a neutron capture network that includes the most recent cross-section measurements as well as the solar abundance data by Lodders, Palme & Gail (2009, Section 2). The AGB models employed in this work have been outlined by Bisterzo et al. (2010, 2014).

In Sections 3 and 4, we discuss the impact of the ^{13}C(α, n)^{16}O and ^{22}Ne(α, n)^{25}Mg uncertainties on the branches of the main component.

Relevant branches of the *s*-path and their influence on the *s*-nuclides are analysed in Section 5. We distinguish the *s*-only isotopes in different classes, according to the characteristics of the related branchings. First, unbranched *s*-only isotopes (e.g. ^{100}Ru, ^{104}Pd, ^{110}Cd, ^{116}Sn, ^{124}Te, ^{150}Sm, ^{160}Dy, and ^{198}Hg) are useful to constrain the main component (Section 5.1). Secondly, we address branchings where the decay of the unstable branch point isotopes exhibits no effect of the *s*-process temperature (e.g. ^{96}Mo, which is sensitive to the branch at ^{95}Zr) or where the half-lives are essentially independent of temperature. These branchings may provide information on the *s*-process neutron density (e.g. ^{170}Yb, partially regulated by ^{169}Er; ^{142}Nd, marginally affected by ^{142}Pr; ^{186}Os, which mainly depends on the branch at ^{185}W; ^{192}Pt, influenced by ^{192}Ir; see Section 5.2). Thirdly, branchings initiated by decays with pronounced dependences on temperature and/or electron density may be interpreted as *s*-process thermometers (e.g. ^{134}Ba, owing to the branch at ^{134}Cs; ^{152,154}Gd, strongly sensitive to ^{151}Sm and ^{154}Eu; ^{176}Lu, which has a short-lived isomer; ^{204}Pb, because of the branch at ^{204}Tl; Section 5.3) or indicators of the turnover time-scale of convective mixing during TP (e.g. ^{128,130}Xe, ^{164}Er, ^{180}Ta$^{\rm m}$; Section 5.4). Each of the three classes is illustrated in detail by a few selected examples: ^{150}Sm, adopted to normalize the *s*-distribution (Section 5.1.1), as well as ^{96}Mo and ^{170}Yb (Sections 5.2.1 and 5.2.2), ^{134}Ba (Section 5.3.1) and ^{180}Ta$^{\rm m}$ (Section 5.4.1), which are most sensitive to uncertainties related to the cross-sections and β-decay rates of the involved branch point nuclei. Other branchings are briefly summarized, referring to the complete discussion in Appendix B (Supporting Information).

In Apppendix C (Supporting Information), we describe the effect of the ^{13}C(α, n)^{16}O, ^{22}Ne(α, n)^{25}Mg and ^{22}Ne(α, γ)^{26}Mg uncertainties on two AGB models (a 3 M$_{\odot}$ model at [Fe/H] = −1 and a half-solar metallicity 5 M$_{\odot}$ model), which are selected as representative of a more extended range of stars than usually adopted for the main component.

An overview of the results is provided in Section 6.

2 UPDATED SOLAR MAIN COMPONENT

Despite the main component does not provide a realistic description of the solar *s*-distribution between A = 90 and 204, it still represents a useful approximation to investigate the effect of nuclear uncertainties of *s*-isotopes in this atomic mass range.

As shown by Arlandini et al. (1999), the ‘stellar’ main component is obtained as the averaged yields between two AGB models with initial masses of 1.5 and 3 M$_{\odot}$ at half-solar metallicity. The *s*-process nucleosynthesis is computed with the post-process method described by Gallino et al. (1998), which is based on input data of full evolutionary FRANEC models by Straniero et al. (1997, 2003), like the temporal history of the temperature and density gradients during the convective TPs, the number of TPs, the mass of the H shell and He-intershell, the overlapping factor and the residual mass of the envelope.

In both AGB models, the ^{22}Ne(α, n)^{25}Mg reaction operates in a similar range of temperatures ($T_8 \sim 2.5$–3). However, the $M = 3$ M$_{\odot}$ model achieves $T_8 \sim 3$ for the last 16 TPs, while the $M = 1.5$ M$_{\odot}$ model for the last eight TPs. The marginal activation of the ^{22}Ne(α, n)^{25}Mg neutron burst mainly occurs in the advanced TPs for a rather short time-scale (∼6 yr).

Most of the *s*-process nucleosynthesis takes place radiatively during the interpulse phases via the ^{13}C(α, n)^{16}O neutron source, which lasts for 3–6 × 10^4 yr (this time decreases with increasing pulse number). We assume a single ^{13}C-pocket profile close to case ST described by Gallino et al. (1998). The case ST ^{13}C-pocket contains 5 × 10^{-6} M$_{\odot}$ of ^{13}C and 2 × 10^{-7} M$_{\odot}$ of ^{14}N, and extends in mass for ∼1 × 10^{-3} M$_{\odot}$ (∼1/10 of the typical mass involved in a TP).

The mass-loss is estimated with the Reimers formula (Reimers 1977) with the parameter $\eta = 0.3$ for 1.5 M$_{\odot}$ and $\eta = 1$ for 3 M$_{\odot}$. This allows the occurrence of 19 and 25 TPs with TDU, respectively. Updated opacities and a revised luminosity function of Galactic carbon stars (Lederer& Aringer 2009; Guandalini & Cristallo 2013) suggest a more efficient mass-loss than the one adopted in our models. This significantly reduces the number of TDUs (e.g. ∼15 TDU for the above models; Cristallo et al. 2011). To this purpose, note that the overall *s*-yields of our AGB models are marginally influenced by the contribution of the *s*-abundances predicted in the envelope for TDU numbers higher than 15. Moreover, the normalization of the average *s*-yields to that of ^{150}Sm allows us to overcome some of the major uncertainties of AGB stellar models (e.g. the efficiency of the TDU, the mass-loss, the number of TPs), which would otherwise dominate the *s*-process predictions (see Section 1).

For major details on the AGB models employed, we refer to Bisterzo et al. (2010, 2014).

The neutron capture cross-section network is based on KADoNiS.[3] Different MACS are adopted for ^{20,21,22}Ne by Heil

---

[3] Karlsruhe Astrophysical Data Base of Nucleosynthesis in Stars, website: http://www.kadonis.org/, version KADoNiSv0.3.

et al. (2014), ^{24,25,26}Mg by Massimi et al. (2012), ^{41}K and ^{45}Sc by Heil et al. (2009), ^{58,62,63}Ni by Žugec et al. (2014) and Lederer et al. (2013, 2014), ^{64,70}Zn by Reifarth et al. (2012), ^{80,82,83,84,86}Kr by Mutti et al. (2005), ^{85}Kr by Raut et al. (2013), ^{92,94,96}Zr by Tagliente et al. (2010, 2011a,b), ^{93,95}Zr by Tagliente et al. (2013) and Lugaro et al. (2014b), ^{136,137}Cs by Patronis et al. (2004), ^{148,149}Pm by Reifarth et al. (2003), ^{152,154}Eu by Best et al. (2001), the p-only ^{180}W by Marganiec et al. (2010), ^{186,187,188}Os by Mosconi et al. (2010), ^{192,194,195,196}Pt by Koehler & Guber (2013) and their theoretical evaluation of the ^{192}Ir MACS.

For a few heavy isotopes, the stellar temperatures are high enough for a significant population of low-lying nuclear excited states, which modify the neutron capture cross-sections measured in laboratory. These effects are considered in the stellar MACS with the so-called stellar enhancement factor (SEF), which accounts of the stellar average over the thermally populated states and the laboratory cross-section. The SEF estimated by Bao et al. (2000) are updated with those recommended by KADoNiS. An exception is ^{187}Os, for which we have adopted Fujii et al. (2010), who studied the inelastic channel of the neutron capture cross-section of ^{187}Os and employed a Hauser–Feshbach statistical model theory to obtain a reliable estimate of the SEF.

The state of the art of all MACS at $kT = 30$ keV versus atomic mass is shown in Fig. 1 (*top panel*). We distinguish between experimental measurements (*small dots*) and theoretical evaluations (*big circles*). Updated MACS with respect to KADoNiS are indicated by *big squares* (experimental measurements) or *triangles* (theoretical evaluations). The *lower panel* of Fig. 1 represents the related percentage MACS uncertainties.

As outlined by Käppeler et al. (2011), most of the MACS involved in the nucleosynthesis of stable isotopes heavier than $A \sim 90$ are known with an accuracy $\lesssim$5 per cent. Uncertainties of ∼10 per cent are evaluated for ^{104}Pd (10 per cent), ^{139}La (9.6 per cent), ^{159}Tb (9.5 per cent; near the *s*-only isotope ^{160}Dy), ^{166,167,168}Er (10 to 13 per cent), ^{200}Hg (10 per cent), ^{209}Bi (11.7 per cent).

Among the unstable isotopes, the largest MACS uncertainties are quoted for ^{85}Kr (∼50 per cent; recently evaluated from the inverse ^{86}Kr(γ, n)^{85}Kr reaction and from the ^{86}Kr(γ, γ') measurement by Raut et al. 2013), ^{86}Rb (∼80 per cent), ^{95}Zr (up to a factor of 2 uncertainty, Lugaro et al. 2014b), ^{141}Ce and ^{142}Pr (∼40 per cent). Other unstable isotopes with uncertainties from 15 to 25 per cent are ^{79}Se (important for the weak *s*-process component), ^{81}Kr, ^{99}Mo, ^{103}Ru, ^{110}Ag, ^{115}Cd, ^{147}Nd, ^{160}Tb, ^{170}Tm, ^{179,182}Ta, ^{181}Hf, ^{186}Re, ^{191}Os, ^{192}Ir, ^{193}Pt, ^{198}Au, ^{203}Hg, ^{204}Tl, ^{205}Pb.

The solar main component is shown in Fig. 2. We examine the *s*-production factors in the He-intershell (corresponding to the overabundances with respect to the solar-scaled initial values given in mass fractions 'X_i') of isotopes with $A > 80$ normalized to the unbranched *s*-only nucleus ^{150}Sm.

A plausible reproduction of *s*-only isotopes heavier than $A = 90$ (full circles) is obtained within the solar abundance uncertainties quoted by Lodders et al. (2009). Variations with respect to previous results by Bisterzo et al. (2011) and Käppeler et al. (2011) partly derive from new solar abundances by Lodders et al. (2009) and partly from updates in the nuclear reaction network. Among the nuclides with $A > 90$, a noteworthy variation is the increased solar abundance of Hg estimated by Lodders et al. (2009, +35 per cent), which reduces the ^{198}Hg solar *s*-contribution by Käppeler et al.

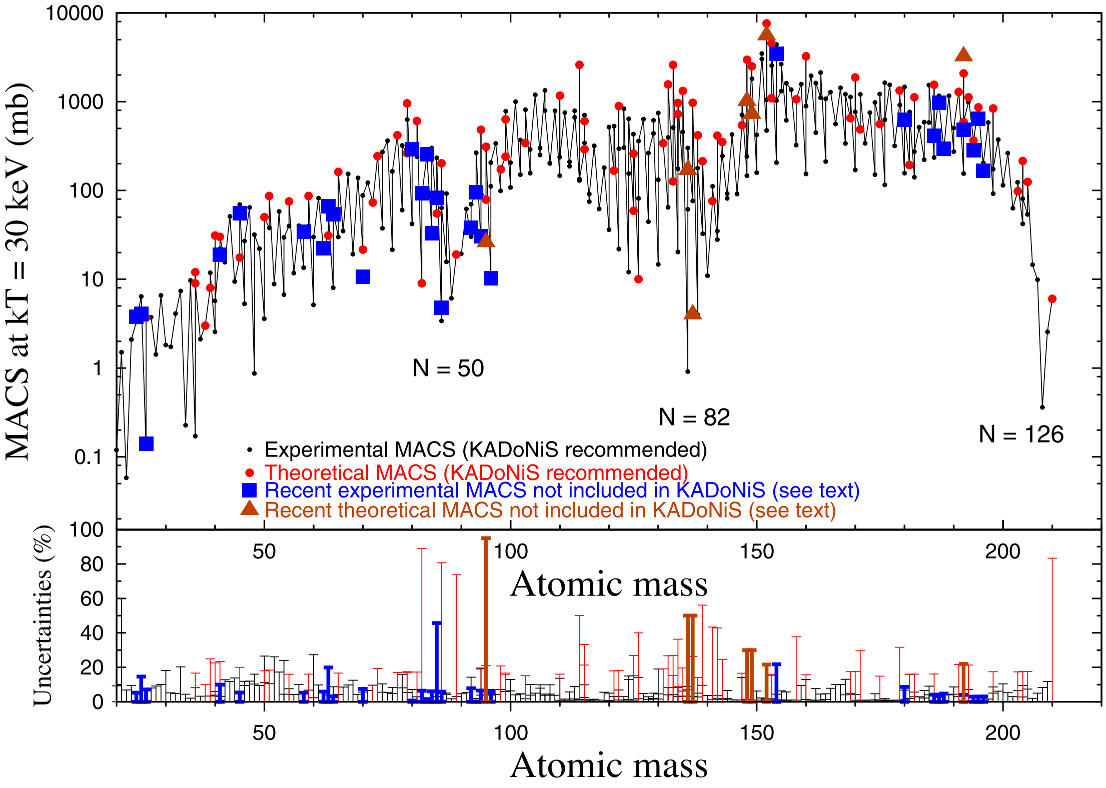

Figure 1. Top panel: stellar (n, γ) cross-sections at 30 keV for nuclides with $A \geq 20$. The compilation is taken from the KADoNiS data base (v0.3): small dots and big circles refer to experimental and theoretical MACS, respectively. Recent MACS not included in KADoNiS, but considered in this work are indicated by squares (experimental measurements) and triangles (theoretical evaluations); see text for details. Neutron-magic numbers at $N = 50$, 82 and 126 are highlighted. Bottom panel: MACS uncertainties at 30 keV. Colours of error bars are the same as in the top panel.

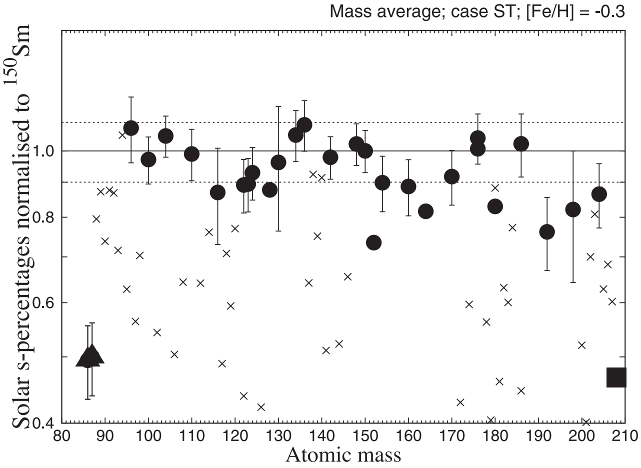

Figure 2. The solar main component versus atomic mass is reproduced by assuming an ST ^{13}C-pocket, and by averaging between AGB models with initial masses of $M = 1.5$ and $3\,M_\odot$ at half-solar metallicity. In this figure, the *s*-production factors are normalized to that of the unbranched *s*-only nucleus ^{150}Sm. The *s*-production factors in the He-intershell (given in mass fraction 'X_i' over the solar-scaled initial values) correspond to the material cumulatively mixed with the envelope by the recurrent TDU episodes and eventually dispersed in the interstellar medium by efficient stellar winds. Different symbols are used for ^{86,87}Sr (which receive additional *s*-contributions, e.g. the weak component in massive stars), and for ^{208}Pb, ~50 per cent of which is produced by low-mass, low-metallicity AGB stars (strong *s*-process). The error bars displayed for the *s*-only isotopes account for the uncertainties of the solar abundances by Lodders et al. (2009). Note that the solar uncertainties are not shown for ^{128}Xe, ^{152}Gd, ^{164}Er, and ^{180}Ta^{m} because they receive additional non-negligible contributions from the (ν)*p*-process by SNIa and SNII (e.g. Rauscher et al. 2002; Pignatari et al. 2013a; Travaglio et al. 2015). The solid line corresponds to a 100 per cent contribution from main component, dashed lines represent 10 per cent of uncertainty.

(2011) from ~100 to 82 per cent. The slightly larger solar Sn uncertainty estimated by Lodders et al. (2009, from 10 per cent by Anders & Grevesse 1989 to 15 per cent) agrees better with the *s*-prediction for ^{116}Sn, although the solar abundance is still 13 per cent higher. Note that the solar Nb and Xe values estimated by Kashiv et al. (2006) and Reifarth et al. (2002) were already considered in Käppeler et al. (2011).

The updated network produces small variations (<5 per cent) among the *s*-only isotopes. Differences larger than ~10 per cent are obtained for ^{164}Er and ^{180}Ta^{m}, where the already ascertained dominant *s*-process contributions (Best et al. 2001; Wisshak et al. 2001) have been increased.

(i) The *s*-contribution of solar ^{164}Er is enhanced by 8 per cent (from 74 to 82 per cent), because a smaller SEF is evaluated for the MACS of ^{164}Er (the old SEF = 1.24 at 30 keV estimated by Bao et al. 2000 is reduced to 1.08 by KADoNiS).

(ii) ^{180}Ta^{m} increases from 75 to 82 per cent (+7 per cent), mostly due to a decreased SEF of the MACS for ^{180}Ta^{m} (from SEF = 0.96 at 30 keV by Bao et al. 2000 to 0.87 by KADoNiS).

Starting from these updated results, we analyse in the following sections the effect of the two AGB neutron source uncertainties on the *s*-distribution and discuss the consequences of the MACS and β-decay rate uncertainties of the most relevant branching points of the main component.

Recently, theoretical analyses by Rauscher et al. (2011) and Rauscher (2012) showed that the SEF correction can cause larger MACS uncertainties than assumed so far. This holds especially for cases, where the (experimentally measured) ground state cross-section constitutes only a minor fraction of the MACS. If the ground state contribution, expressed by a new factor *X*, is close to unity, the uncertainty of the stellar rate is directly connected to the experimental one; otherwise, the uncertainty of stellar rate may be larger than that of the experimental measurement.

The theoretical uncertainties discussed by Rauscher et al. (2011) are not included in this work, because they should be considered as upper limits of future more realistic analyses, which need to be carried out individually for each nucleus, by accounting of all available nuclear details. The situation is even more challenging when the experimental rate is inferred from the inverse neutron capture reaction, (γ,n) (e.g. the case of ^{185}W; Rauscher 2014). On the base of the branches analysed in Section 5 and in Appendix B (Supporting Information), we highlight outstanding isotopes that would need specific theoretical investigations in Section 6.

3 UNCERTAINTY OF THE ^{13}C(α, N)^{16}O NEUTRON SOURCE

As anticipated in Section 1, the ^{13}C(α, n)^{16}O rate is the dominant neutron source in low-mass AGBs and shapes the overall *s*-abundance component. It burns radiatively during the interpulse periods in the top layers of the He-intershell when the temperature reaches $T_8 \sim 0.8$–1.0. Under these conditions, the ^{13}C(α, n)^{16}O rate is extremely small (10^{-14}–10^{-13} cm^3 mol^{-1} s^{-1}) and, therefore, not yet accessible to direct measurements in terrestrial laboratories, owing to the high background signals induced by cosmic γ-rays. Current reaction rates have been determined by extrapolation of direct measurements performed at energies higher than 270 keV, far from the Gamow window at 140–230 keV where the ^{13}C(α, n)^{16}O reaction is effective (see e.g. Drotleff et al. 1993). This entails an unknown influence of broad sub-threshold states. A major impact is expected from the contribution of the sub-threshold resonance due to the $J^\pi = 1/2^+$ state in ^{17}O at 6.356 MeV ($E_\alpha^{\rm lab} = -3$ keV), while minor effects are expected due to sub-threshold resonances at 5.939 MeV ($J^\pi = 1/2^-$; $E_\alpha^{\rm lab} = -547$ keV) and 5.869 MeV ($J^\pi = 3/2^+$; $E_\alpha^{\rm lab} = -641$ keV).

Past analyses showed large uncertainties at 8 keV (up to a factor of 3) owing to the unexplored contribution of the 6.356 MeV state (see e.g. Caughlan & Fowler 1988; Angulo et al. 1999). More recent evaluations by Heil et al. (2008b) and Guo et al. (2012) are in reasonable agreement and provide a significantly reduced uncertainty (down to ~20–30 per cent, in the AGB energy range of interest). Later, La Cognata et al. (2013) attained an accuracy of 15 per cent for the ^{13}C(α, n)^{16}O rate by means of the Trojan horse method, which allows one to study reactions of astrophysical interest free of Coulomb suppression and electron screening at astrophysical energies with no need for extrapolation. This method clearly displays the presence of the sub-threshold resonance corresponding to the 6.356 MeV ^{17}O state. Their rate is about 35 per cent higher than that by Heil et al. (2008b), still in agreement within uncertainties with most of the results in literature at $T_8 \sim 1$.

In Table 1, we provide a summary of the most relevant ^{13}C(α, n)^{16}O rates found in literature at $T_8 = 1$.

In our AGB models, we adopt the ^{13}C(α, n)^{16}O rate by Denker et al. (1995), which is pretty close to the results by Heil et al. (2008b) and Guo et al. (2012).

We carried out two extreme tests in order to analyse the effect of the ^{13}C(α, n)^{16}O uncertainty on the main component.

Table 1. The ^{13}C(α, n)^{16}O rate at $T = 1 \times 10^8$ K (in units of 10^{-14} cm^3 mol^{-1} s^{-1}) determined by Caughlan & Fowler (1988), Denker et al. (1995), Kubono et al. (2003), Johnson et al. (2006), Heil et al. (2008b), Guo et al. (2012), NACRE II (Xu et al. 2013b) and La Cognata et al. (2013). Additional studies are not listed explicitly, but found ^{13}C(α, n)^{16}O rates within these ranges.

Reference	Rate (10^{-14} cm^3 mol^{-1} s^{-1})	Lower limit	Upper limit
Caughlan & Fowler (1988)	2.58	–	–
Kubono et al. (2003)	2.02	1.49	2.54
Johnson et al. (2006)	2.64	2.11	3.30
NACRE II	4.86	3.62	6.48
Denker et al. (1995)	4.32	–	–
Heil et al. (2008b)	4.6	3.6	5.6
Guo et al. (2012)	4.19	3.46	4.90
La Cognata et al. (2013)	6.20	5.32	7.13

(i) *Test* 1 – adopted ^{13}C(α, n)^{16}O rate multiplied by a factor of 2, close to the upper limit by La Cognata et al. (2013).

(ii) *Test* 2 – adopted ^{13}C(α, n)^{16}O rate divided by a factor of 3, close to the lower limit by Kubono et al. (2003).

The results of the two tests are shown in Fig. 3 for isotopes with A > 80. We focus on *s*-only isotopes for clarity (*circles*). The ratio of the results obtained in the tests and with the adopted ^{13}C(α, n)^{16}O rate are plotted in the *upper* and *lower panels* together with the 10 per cent limits indicated by dashed lines.

We see that the main component is marginally affected by both tests: variations are smaller than 1 per cent for the *s*-only isotopes with $A > 90$ and smaller than 3 per cent between $A = 80$ and 90.

Significant changes were obtained, however, for the two neutron-magic nuclei ^{86}Kr and ^{87}Rb (represented by *crosses*), because the branching at ^{85}Kr is partially activated during the ^{13}C(α, n)^{16}O phase. For a comprehensive discussion, see Appendix B (Supporting Information). We note, however, that both isotopes receive a small contribution from AGB stars: only ~16 and ~18 per cent of solar ^{86}Kr and ^{87}Rb are produced by the main component, respectively.

In our AGB models with initial masses 1.5 and 3 M$_\odot$ and half-solar metallicity, the amount of ^{13}C in the pocket assumed for case ST burns radiatively during the interpulse even by reducing the ^{13}C(α, n)^{16}O rate by a factor of 3. Only a ^{13}C mass fraction negligible for the *s*-process is ingested in the next convective TP.

Otherwise, when a substantial amount of ^{13}C is ingested in the subsequent TP, it burns at the bottom of the convective shell (at $T_8 \sim 1.6$) in a very short time-scale (of the order of few years), producing enhanced neutron densities of up to $\sim 10^{10-11}$ cm^{-3}. A new generation of AGB models available at the FRUITY data base by Cristallo et al. (2009, 2011) experiences a partial convective burning of ^{13}C during the first (and second) TP(s). This mainly occurs in low-mass metal-rich AGB models and influences the abundances of a few neutron-rich isotopes during the first TPs (e.g. ^{86}Kr, ^{87}Rb, ^{96}Zr; and radioactive nuclides as ^{60}Fe, see Cristallo et al. 2006, 2011).

Actually, the recent measurement by La Cognata et al. (2013) suggests that the ^{13}C(α, n)^{16}O rate adopted in our models must be increased by 40 per cent, rather than decreased (see Table 1). In this case, the ingestion of ^{13}C into TPs is strongly reduced.

Despite the main component presented in this work is marginally influenced by the uncertainty of the ^{13}C(α, n)^{16}O rate, AGB predictions in general may show larger sensitivity, when e.g. a different amount of ^{13}C is assumed in the pocket, or a lower initial metallicity is adopted. Moreover, the physical characteristics of different stellar models employed in the nucleosynthesis calculations may influence the effect of the ^{13}C(α, n)^{16}O rate. For instance, recent low-mass AGB models are characterized by more efficient TDU episodes (see the discussion in Straniero et al. 2006[4]). In particular, the first TDU occurs at the very beginning of the TP-AGB phase, when the core mass is rather small and, in turn, the temperature developed in the He-rich intershell during the interpulse period is lower (Cristallo et al. 2009). In this case, a non-negligible amount of ^{13}C that survives after the interpulse is engulfed in the convective zone generated by the subsequent TP and burns at relatively high temperature. For example, in 1.8 M$_\odot$ models by Lugaro et al. (2012) and Guo et al. (2012), the convective burning of the partial ^{13}C ingested in the TPs affects *s*-predictions up to Pb. This effect may even become dominant for lower mass AGB models (e.g. in $M^{\rm AGB}_{\rm ini} = 1.25$ M$_\odot$ models of half-solar metallicity, the ^{13}C neutron source burns convectively rather than radiatively; Raut et al. 2013).

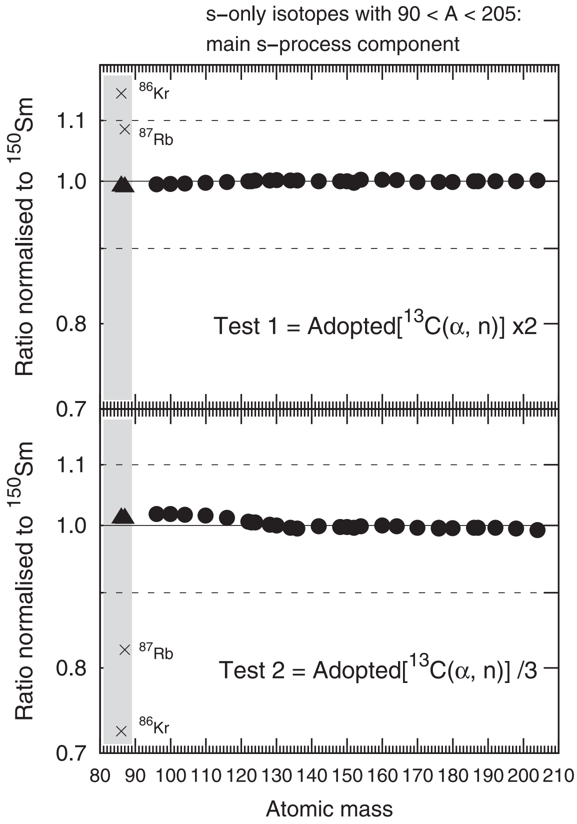

Figure 3. Ratios between the main component obtained with a two times higher and a three times lower ^{13}C(α, n)^{16}O rate than our adopted rate shown in Fig. 2 (Test 1 and Test 2 corresponding to the top and bottom panels). We focus on *s*-only isotopes for clarity. The shaded area between $80 < A \lesssim 90$ indicates the atomic mass region affected by additional *s*-contributions (e.g. the weak *s*-process in massive stars; IMS AGB stars, see Appendices B and C, Supporting Information). The two neutron-magic nuclei ^{86}Kr and ^{87}Rb, which exhibit the largest variations, are marked by crosses (see text). A complete version of this figure (which includes all isotopes from $90 \le A \le 210$) is given in Appendix A (Supporting Information).

---

[4] A more efficient TDU is required to reproduce the observed luminosity function of the carbon stars in the Milky Way and in the Magellanic Clouds (Cristallo et al. 2011; Guandalini & Cristallo 2013).

4 UNCERTAINTY OF THE ^{22}NE(α, N)^{25}MG NEUTRON SOURCE AND THE ^{22}NE(α, γ)^{26}MG RATE

While the ^{13}C(α, n)^{16}O neutron source determines the overall shape of the main component, the contribution of the ^{22}Ne(α, n)^{25}Mg reaction affects the *s*-only isotopes close to branching points.

For the ^{22}Ne(α, n)^{25}Mg reaction, the centre-of-mass energy region of interest to the *s*-process is $E_{\rm c.m.}$ = 300 to 900 keV. At these low energies, direct ^{22}Ne(α, n)^{25}Mg measurements are limited by cosmic γ-ray background because the cross-section rate is extremely small. The lowest well studied $J^\pi = 2^+$ resonance at ∼832 keV, which dominates the ^{22}Ne(α, n)^{25}Mg rate (Drotleff et al. 1993), lies above the relevant astrophysical energies. Theoretical extrapolations of the ^{22}Ne(α, n)^{25}Mg reaction measured at higher energies may be affected by the unknown influence of low-energy resonances just below the neutron threshold.

The resonances affecting the (α, n) and (α, γ) rates of ^{22}Ne correspond to different levels in the compound nucleus. First investigations derived a large ^{22}Ne(α, n)^{25}Mg uncertainty because of the influence of a possible resonance at ∼635 keV with assigned natural spin-parity $J^\pi = 1^-$ (e.g. NACRE; Käppeler et al. 1994; Angulo et al. 1999; Jaeger et al. 2001; Koehler 2002). Successively, Longland et al. (2009) determined the energy and quantum numbers of excited states in ^{26}Mg through a nuclear resonance fluorescence experiment and demonstrated that the corresponding level at an excitation energy of E_x = 11 154 keV has unnatural parity $J^\pi = 1^+$, contrary to the previous spin-parity assignment. Because both ^{22}Ne and ^{4}He have $J^\pi = 0^+$, by angular momentum selection rules only natural-parity (0^+, 1^-, 2^+, etc.) states in ^{26}Mg can participate in the ^{22}Ne(α, n)^{25}Mg reaction, thus excluding the $J^\pi = 1^+$ resonance. Nevertheless, the ^{22}Ne(α, n)^{25}Mg rate may be affected by the possible contribution of other unknown low-threshold states of natural parity (Ugalde et al. 2007; deBoer et al. 2010). Moreover, if yet unknown low-energy resonances have a strong influence on the ^{22}Ne(α, γ)^{26}Mg rate, the ^{22}Ne(α, γ)^{26}Mg and ^{22}Ne(α, n)^{25}Mg reactions may compete during TPs, further affecting the neutron production in AGB stars (see e.g. IMS stars; Karakas et al. 2006).

The recent theoretical estimate by Longland et al. (2012) based on a Monte Carlo evaluation suggests a much smaller ^{22}Ne(α, n)^{25}Mg uncertainty (∼20 per cent).

In previous AGB models (e.g. Bisterzo et al. 2010, 2011), we have adopted the lower limit of the ^{22}Ne(α, n)^{25}Mg and ^{22}Ne(α, γ)^{26}Mg rates by Käppeler et al. (1994). These rates were evaluated by neglecting the resonance contribution at 633 keV. At $T_8 = 3$, the ^{22}Ne(α, n)^{25}Mg rate was about 50 per cent higher than that recommended by Jaeger et al. (2001), close to the upper limit by Longland et al. (2012).

In Table 2, we summarize some of the most significant results achieved in the estimate of the ^{22}Ne(α, n)^{25}Mg and ^{22}Ne(α, γ)^{26}Mg rates for the maximum temperature at the bottom of the advanced TPs in the AGB models adopted here ($T_8 = 3$).

We have calculated the rates of the ^{22}Ne(α, n)^{25}Mg and ^{22}Ne(α, γ)^{26}Mg reactions ('This work' in Table 2; see also Fig. 4) by accounting for the most recent studies of all known (directly and/or indirectly detected) resonances as well as nuclear data available in literature.

In particular, we adopted the rates calculated on the basis of experimentally detected levels, i.e. mainly on the basis of the values of Jaeger et al. (2001). For the ^{22}Ne(α, γ)^{26}Mg rate, we added the states which have an indirect determination of the α width using the ^{22}Ne(^{6}Li, d) reaction (Giesen et al. 1993). In the temperature

Table 2. The ^{22}Ne(α, n)^{25}Mg and ^{22}Ne(α, γ)^{26}Mg rates at 3 × 10^8 K (in unit of 10^{-11} cm^3 mol^{-1} s^{-1}) estimated by Caughlan & Fowler (1988), NACRE (Angulo et al. 1999), Käppeler et al. (1994), Jaeger et al. (2001), Longland et al. (2012). The newly evaluated values are labelled with 'This work' (see text for explanations). We distinguish between experimental measurements (exp) and theoretical evaluations (th).

Reference	Recommended rate (10^{-11} cm^3 mol^{-1} s^{-1})	Lower limit	Upper limit
^{22}Ne(α, n)^{25}Mg rate:			
Caughlan & Fowler (1988); (th)	1.86	–	–
NACRE; (th)	4.06	3.37	192.0
Käppeler et al. (1994); (exp)	**9.09**	**4.14**	**14.4**
Jaeger et al. (2001); (exp)	**2.69**	**2.63**	**3.20**
Longland et al. (2012); (th)	**3.36**	**2.74**	**4.15**
This work; (th)	**2.24**	**1.99**	**2.92**
^{22}Ne(α, γ)^{26}Mg rate:			
Caughlan & Fowler (1988); (th)	0.46	–	–
NACRE; (th)	2.56	0.59	20.30
Käppeler et al. (1994); (exp)	**1.22**	**0.81**	**1.63**
Longland et al. (2012); (th)	**1.13**	**0.93**	**1.38**
This work; (th)	**0.80**	**0.72**	**2.62**

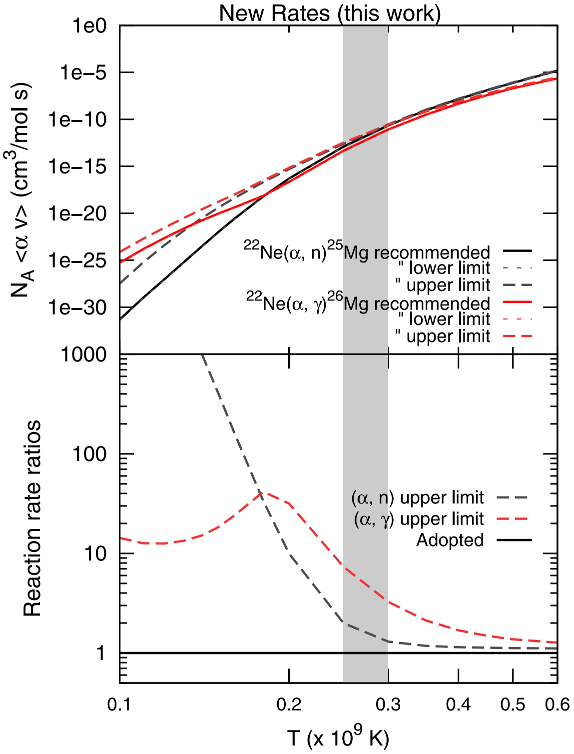

Figure 4. Top panel: new evaluated values of the ^{22}Ne(α, n)^{25}Mg and ^{22}Ne(α, γ)^{26}Mg rates with black and red lines, respectively. The difference between lower and recommended rates is almost unnoticeable (about 10 per cent at all temperatures; dotted lines). Our upper rates are shown by dashed lines. See text for details on the computed uncertainties. Bottom panel: the uncertainty bands for the ^{22}Ne(α, n)^{25}Mg and ^{22}Ne(α, γ)^{26}Mg reactions. The uncertainties are the result of upper-limit resonance contributions and of resonance strength uncertainties. The shaded areas at T_8 = 2.5–3 indicates the temperature range reached during TPs by low-mass AGB stars. Explicit values of both rates at T_8 = 3 are given in Table 2.

range of low-mass AGB stars (T_8 = 2.5–3), the ^{22}Ne(α, n)^{25}Mg recommended value is about a factor of 2 lower than that adopted in our models so far, while the recommended ^{22}Ne(α, γ)^{26}Mg rate is essentially unchanged.

We have also determined *lower* and *upper values* of both rates considering additional resonances in order to investigate their potential impact (see Fig. 4, bottom panel). The *lower limit* is determined by the lower experimental limit of the 703 keV resonance (11 per cent). This reduces the recommended rates by about 10 per cent at all temperatures. For the *upper rate*, we introduced all the known (but not directly measured) states below the 703 keV resonance, adopting a spectroscopical factor of 0.01, which represents a conservative upper limit. Moreover, we have estimated a possible larger effect due to one of the low-energy states. We then concentrated on the lower energy states, which give substantial contributions to the reaction rate for $T < 0.3$ GK. This was done to investigate the influence of possible α cluster states in ^{26}Mg. These states could have spectroscopic factors as large as 0.1. Larger values are unlikely because they should have been observed in α transfer reactions. For the (α, γ) reaction, we identified two states, one above (568 keV) and one below (433 keV) the neutron threshold. Also for the (α, n) reaction, there are two states: one at 497 keV and another at 548 keV. This corresponds to an increase of the recommended ^{22}Ne(α, n)^{25}Mg recommended rate by a factor of 2 at $T_8 = 2.5$ and by +30 per cent at $T_8 = 3$. The recommended ^{22}Ne(α, γ)^{26}Mg rate increases up to a factor of 7 at $T_8 = 2.5$ and by a factor of 3 at $T_8 = 3$ (see dashed lines in Fig. 4, bottom panel). Note that in network calculation one should not use the upper rate for both ^{22}Ne(α, n)^{25}Mg and ^{22}Ne(α, γ)^{26}Mg reactions at the same time because the change of spectroscopic factors has influence on both rates.

Based on the above results, we have updated the solar main component discussed in Section 2 with the recommended ^{22}Ne(α, n)^{25}Mg and ^{22}Ne(α, γ)^{26}Mg rates (see Fig. 5; *filled circles*). By comparing these revised results with the previous *s*-distribution displayed in Fig. 2, major variations are shown close to the branches of the *s*-path.

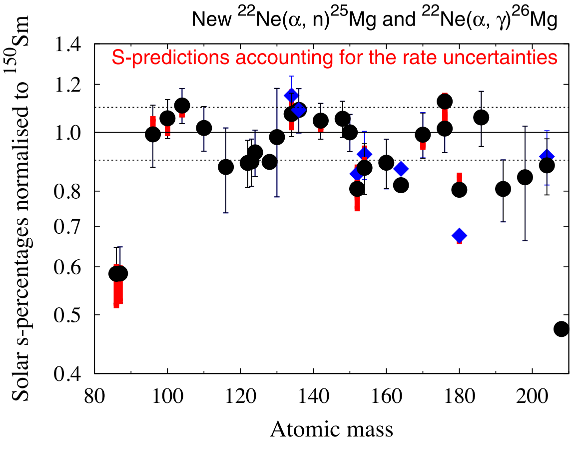

Figure 5. The solar main component versus atomic mass (as shown in Fig. 2) obtained with the recommended ^{22}Ne(α, n)^{25}Mg and ^{22}Ne(α, γ)^{26}Mg rates (see Fig. 4). We focus on *s*-only isotopes for clarity (filled circles). Also ^{86,87}Sr (which receive additional *s*-contributions) and ^{208}Pb (not an *s*-only nuclide) are displayed for completeness. Thin error-bars account for the uncertainties of the solar abundances by Lodders et al. (2009). Thick bars are obtained by including the uncertainties of the recommended rates discussed in the text (lower and upper limits) and shown in Fig. 4. We indicate the results of an improved treatment of the half-life of a few key isotopes strongly sensitive to temperature (and electron density), which influence the nearby isotopes (^{134,136}Ba, ^{152,154}Gd, ^{164}Er, ^{180}Ta$^{\rm m}$ and ^{204}Pb; filled diamonds, see text).

The impact of the uncertainties evaluated for the recommended ^{22}Ne(α, n)^{25}Mg and ^{22}Ne(α, γ)^{26}Mg rates (Fig. 4) has a rather small effect on the *s*-distribution (see thick bars in Fig. 5). The abundances of *s*-only isotopes are reproduced within the solar uncertainties.

However, it should be noted that the several ambiguities remaining in the nuclear data for the ^{22}Ne + α reaction rates need to be resolved. Indeed, the theoretical ^{22}Ne(α, n)^{25}Mg and ^{22}Ne(α, γ)^{26}Mg rates presented in this work (and all estimations given in literature as well) are based on old experimental measurements (e.g. Jaeger et al. 2001) and the uncertainties may be underestimated. The presence of low-energy unknown states, which have been identified in several indirect experiments, makes the evaluation at relevant energy still uncertain. New direct experimental investigations are needed to measure the resonances with higher accuracy.

Future investigations are in progress to shed light on this issue (e.g. via indirect measurements at n_TOF-EAR2; Chiaveri et al. 2012; Massimi et al. 2014; or at accelerator facilities deep underground where the cosmic ray background into detectors is reduced by several orders of magnitude, LUNA[5] and DIANA[6]).

Our post-process AGB models generally adopt constant β-decay rates, which are based on a geometric average of the rates given by Takahashi & Yokoi (1987) at different temperatures (and electron densities) over the convective pulse. Note that this approximation does not affect the prediction of most of the *s*-only branched isotopes, because the β-decay rates of close unstable nuclei are almost constant in the temperature range of the TP, or they do not compete with neutron capture rates. Relevant exceptions are ^{134}Ba, ^{152,154}Gd, ^{164}Er, ^{176}Lu/^{176}Hf, ^{180}Ta$^{\rm m}$, ^{204}Pb: in these cases, the β-decay rates of close unstable isotopes (e.g. ^{134}Cs, ^{151}Sm and ^{154}Eu, ^{164}Ho, ^{176}Lu, ^{180}Ta$^{\rm m}$, ^{204}Tl, respectively) vary by order(s) of magnitude over the large temperature and density gradients that characterize the convective zone ($0.2 \lesssim T_8 \lesssim 3$ and $10 \lesssim \rho \lesssim 10^4$ g cm^{-3}), competing with neutron captures. The above branches require an improved treatment of the β-decay rates over the TP.

The treatment of the branches close to ^{176}Lu/^{176}Hf and ^{180}Ta$^{\rm m}$ was already refined in recent AGB models (see Wisshak et al. 2006b; Heil et al. 2008c). We extend the improvement to the branches close to ^{134}Ba, ^{152,154}Gd, ^{164}Er and ^{204}Pb. We further implement the *s*-prediction of ^{180}Ta$^{\rm m}$, by including the same treatment to nearby branched isotopes (^{179}Ta and ^{179}Hf).

We provide detailed calculations by dividing each TP in 30 convective meshes of constant mass. In each mesh, temperature (and density) can be considered constant during each time step. We follow the production and destruction of the unstable isotopes close to the above *s*-only nuclides in each mesh with the β-decay rates computed at each mesh temperature. The neutron density resulting from the ^{22}Ne(α, n)^{25}Mg reaction is computed in the various meshes at each time step. Neutron densities for an efficient *s*-process are only reached in the bottom region of the convective zone (see Fig. A1, Appendix A, Supporting Information). The abundances resulting in each zone after neutron irradiations are periodically mixed to account for the turnover time of the convective zone (of the order of a few hours).

As shown in Fig. 5, ^{134}Ba, ^{152,154}Gd, ^{164}Er and ^{180}Ta$^{\rm m}$ are mainly affected by the improved treatment of the β-decay rates (see *filled*

---

[5] See Costantini et al. (2009) and references therein; website: http://luna.lngs.infn.it/.

[6] See Lemut et al. (2011).

diamonds); a variation smaller than 5 per cent is displayed by ^{204}Pb. We will provide a more detailed discussion on these branches in Section 5 and Appendix B (Supporting Information).

4.1 Tests of the ^{22}Ne(α, n)^{25}Mg and ^{22}Ne(α, γ)^{26}Mg rates

As discussed in Section 4, future direct experimental measurements of the ^{22}Ne(α, n)^{25}Mg and ^{22}Ne(α, γ)^{26}Mg reaction rates may evidence the presence of low-energy unknown states. Also the contribution of known resonances needs to be determined with high precision.

These considerations encourage us to work in a more conservative range of uncertainty than that estimated in Section 4: starting from our recommended ^{22}Ne(α, n)^{25}Mg and ^{22}Ne(α, γ)^{26}Mg rates (hereafter adopted to compute the reference *s*-distribution; see Fig. 5), we investigate the effects of the following tests on the solar main component:

(i) *Test A* – recommended ^{22}Ne(α, n)^{25}Mg rate multiplied by a factor of 4, close to the recommended value by Käppeler et al. (1994), while the ^{22}Ne(α, γ)^{26}Mg rate is almost unchanged.

(ii) *Test B* – recommended lower limits of the ^{22}Ne(α, n)^{25}Mg and ^{22}Ne(α, γ)^{26}Mg rates.

(iii) *Test C* – recommended ^{22}Ne(α, n)^{25}Mg rate and upper limit for the ^{22}Ne(α, γ)^{26}Mg rate. This test evaluates the competition between (α, γ) and (α, n) rates in AGB models of low initial mass.

In Fig. 6, we show the effect of *Test A* (*upper panel*) and Test B (*lower panel*) on the solar main component of *s*-only isotopes with $A > 80$. In both panels, a 10 per cent uncertainty is indicated by dashed lines. A detailed list of the results of both tests that includes all isotopes with $A \geq 70$ is given in Table A1, (Supporting Information).

Values are obtained by normalizing the *s*-production factors to that of ^{150}Sm in both tests. Note that for ^{150}Sm we obtain an *s*-production factor of X(^{150}Sm)/X$_{\rm ini}$(^{150}Sm) = 1133.9 with the recommended ^{22}Ne(α, n)^{25}Mg and ^{22}Ne(α, γ)^{26}Mg rates. Test A provides X(^{150}Sm)/X$_{\rm ini}$(^{150}Sm) = 1275.5 (+12.5 per cent), and Test B yields X(^{150}Sm)/X$_{\rm ini}$(^{150}Sm) = 1128.4 (−1.0 per cent). The *s*-production of ^{150}Sm increases by +12.5 per cent with increasing the ^{22}Ne(α, n)^{25}Mg by a factor of 4. This difference is independent of any branch (see Section 5.1.1) and affects the entire *s*-process distribution in the same way.

As displayed by Test A, the ^{22}Ne(α, n)^{25}Mg rate mainly affects ^{86,87}Sr, which decrease by ∼30 per cent being regulated by the branches at ^{85}Kr and ^{86}Rb. We remind that the main-component synthesises about half of solar ^{86,87}Sr (see discussion in Appendices B and C, Supporting Information).

Noteworthy variations (∼10–20 per cent) are obtained for ^{96}Mo, ^{134}Ba, ^{142}Nd, ^{152}Gd, ^{170}Yb, and ^{176}Lu. The *s*-prediction to ^{96}Mo is affected by the branch at ^{95}Zr (Sections 5.2.1); the large sensitivity of the branch at ^{134}Cs to neutron density modifies the ^{134}Ba/^{136}Ba ratio (up to 10 per cent; Section 5.3.1); ^{142}Nd is regulated by the branch at ^{141}Ce (Appendix B, Supporting Information); the branches at ^{151}Sm and ^{154}Eu influence the *s* production of $^{152,\,154}$Gd (e.g. variations of 20 per cent of ^{152}Gd; Appendix B, Supporting Information); ^{170}Yb is affected by the branch at ^{170}Tm (10 per cent; Section 5.2.2); finally, the branch at ^{176}Lu modifies the ^{176}Lu/^{176}Hf ratio (see discussion in Appendix B, Supporting Information).

Note that the *s*-contribution to ^{100}Ru and ^{104}Pd also shows important variation, although the branches at ^{99}Mo and ^{103}Ru (with strongly reduced half-lives at stellar temperatures) are only marginally open. In both cases, the ∼16 per cent variation is mainly explained by the cumulative effect of a different *s*-contribution to ^{150}Sm, adopted to normalize the *s*-distribution.

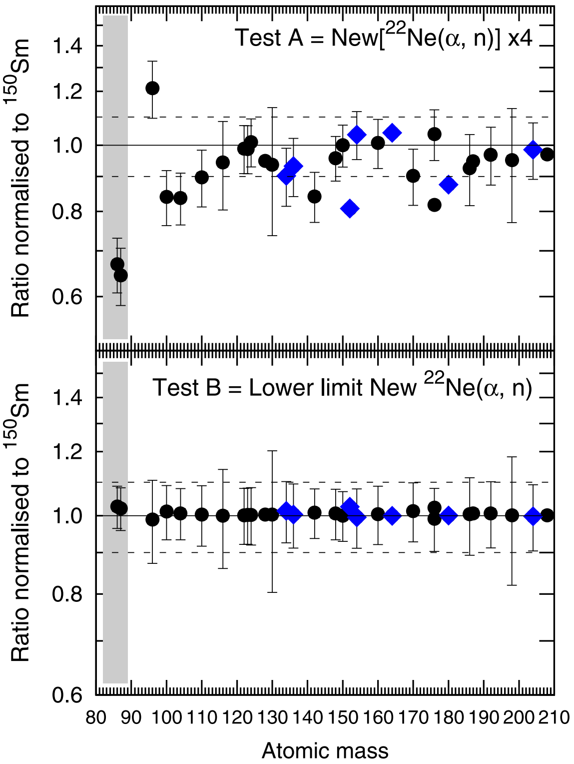

Figure 6. Ratios between the main component obtained with Tests A and B and our results obtained with the recommended ^{22}Ne(α, n)^{25}Mg and ^{22}Ne(α, γ)^{26}Mg rates (Fig 4). We focus on *s*-only isotopes for clarity (filled circles). An improved treatment of the branches close to ^{134}Ba, $^{152,\,154}$Gd, ^{164}Er, ^{180}Ta$^{\rm m}$ and ^{204}Pb is included (filled diamonds). A complete version of this figure (which includes all isotopes from $90 \leq A \leq 210$) is given in Appendix A (Supporting Information). As in Fig. 3, the shaded area between $80 < A < 90$ indicates the atomic mass region affected by additional *s*-contributions.

Other *s*-only isotopes show differences of less than 5 per cent.

A comprehensive description of the most important branchings of the main component is provided in Section 5.

Note that the variations shown by Test B are marginal because our recommended ^{22}Ne(α, n)^{25}Mg rate lies close to a plausible lower limit (∼ −10 per cent; Section 4). Indeed, the dominant effect of the resonance at 800 keV indicates that smaller values are unlikely.

In our AGB models with initial masses 1.5 and 3 M$_\odot$ and half-solar metallicity, the competition between the ^{22}Ne(α, γ)^{26}Mg and ^{22}Ne(α, n)^{25}Mg reactions is marginal: in spite of the rather generous margins considered for the ^{22}Ne(α, γ)^{26}Mg rate, Test C confirms that the effect of the ^{22}Ne(α, γ)^{26}Mg rate for the *s*-abundance distribution is negligible (see Fig. 7).

Appreciable variations are only seen for ^{26}Mg, directly involved in the (α, γ) reaction. Due to its very small MACS (0.126 ± 0.009 mb at 30 keV; Bao et al. 2000), ^{26}Mg is accumulated in the *s*-process.

In stellar models with higher initial mass (e.g. IMS stars), where the temperature at the bottom of the TP increases sufficiently to efficiently activate both ^{22}Ne(α, n)^{25}Mg and ^{22}Ne(α, γ)^{26}Mg reactions, their competition becomes important for the nucleosynthesis of Mg isotopes (see e.g. Karakas et al. 2006; Longland et al. 2012). Above all, the ^{22}Ne(α, n)^{25}Mg rate plays a key role in the production of *s*-isotopes, as the ^{13}C(α, n)^{16}O neutron source is expected to have small or negligible effects in IMS stars (see Section 1).

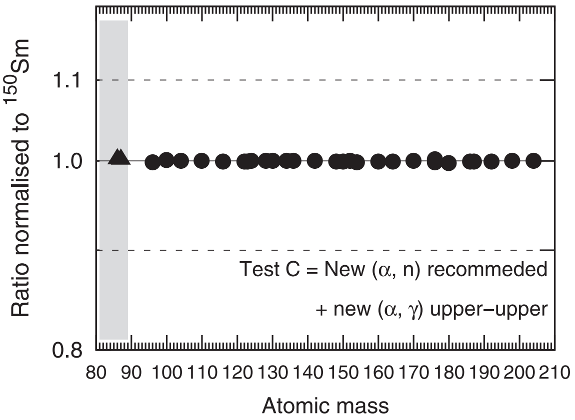

Figure 7. Ratios between the main component obtained with the recommended ^{22}Ne(α, n)^{25}Mg and ^{22}Ne(α, γ)^{26}Mg rates compared to Test C in which the upper limit for the ^{22}Ne(α, γ)^{26}Mg rate is adopted, while the ^{22}Ne(α, n)^{25}Mg reaction is unchanged. Symbols are the same as Fig. 6. A complete version of this figure (which includes all isotopes from $90 \leq A \leq 210$) is given in Appendix A (Supporting Information).

In Appendix C (Supporting Information), we discuss the impact of the ^{22}Ne(α, n)^{25}Mg and ^{22}Ne(α, γ)^{26}Mg rates on two AGB models: a 5 $M_\odot$ model at half-solar metallicity taken as example of IMS stars and a 3 $M_\odot$ model at [Fe/H] $= -1$ chosen as representative of low-metallicity models.

In a 5 $M_\odot$ model at half-solar metallicity, the maximum temperature at the bottom of the convective TPs is $T_8 \sim 3.6$. In this condition, the ^{22}Ne(α, n)^{25}Mg neutron burst efficiently operates, reaching a neutron density of $N_{\rm n} \sim 10^{11}$ cm^{-3}. The whole s-distribution increases by up to a factor of $\sim$2 by including the upper limit of the recommended ^{22}Ne(α, n)^{25}Mg rate, and by one order of magnitude with Test A (recommended [^{22}Ne(α, n)^{25}Mg] × 4). Key neutron-rich isotopes (^{86}Kr, ^{87}Rb, ^{96}Zr) are largely produced being the branches at ^{85}Kr and ^{95}Zr easily open. The impact of the ^{22}Ne(α, γ)^{26}Mg rate on s-isotopes remains rather small ($\lesssim$6 per cent).

In low-mass AGB stars with [Fe/H] < -0.3, the ^{22}Ne(α, n)^{25}Mg uncertainty also produces a larger impact on s-predictions than that observed on the solar main component. For instance, in a 3 $M_\odot$ model at [Fe/H] $= -1$, the maximum temperature at the bottom of the advanced TPs reaches $T_8 = 3.5$. In this case, both ^{22}Ne(α, n)^{25}Mg and ^{13}C(α, n)^{16}O neutron sources operate efficiently. In addition, the s-distribution is largely modified by the lower initial metallicity: as discussed in Section 1, by decreasing the metallicity the abundances of isotopes with neutron magic numbers $N = 50$ and 82 are progressively overcome (thus reducing the whole distribution between $90 \lesssim A \lesssim 130$ and $140 \lesssim A \lesssim 204$, respectively), while ^{208}Pb is mainly produced.

We refer to Appendix C (Supporting Information) for major details.

5 UNCERTAINTIES OF MAJOR BRANCHES OF THE MAIN COMPONENT

We distinguish the s-only isotopes in three classes, according to their related unstable branch point isotopes:

(i) unbranched s-only isotopes (Section 5.1), with unstable isobars having half-lives shorter than a couple of days (thus forbidding neutron captures during TPs);

(ii) s-only isotopes sensitive to neutron density only (Section 5.2), with unstable isobars having half-lives (almost) constant in stellar environments;

(iii) s-only isotopes affected by branch point with unstable isobars having β-decay rates quickly changing under stellar conditions: we distinguish between nuclides sensitive to both neutron density and stellar temperature (and/or electron density; Section 5.3) and nuclides less affected by neutron density, but dominated by stellar temperature and/or electron density gradients during TP (Section 5.4).

5.1 Unbranched *s*-only isotopes

As mentioned in Section 2, a few s-only isotopes of the s-path (^{100}Ru, ^{110}Cd, ^{116}Sn, ^{124}Te, ^{150}Sm, ^{160}Dy; see Arlandini et al. 1999; as well as ^{104}Pd and ^{198}Hg) are marginally affected by nearby branch points with short half-lives. Thus, only a few per cent of the s-path (<3 per cent) bypasses the above s-only nuclides, which become useful constraints for the main component.

5.1.1 The s*-only isotope* ^{150}*Sm*

^{150}Sm is one of the few s-only isotopes that is exposed to the full s-flow, because all branches in the Nd–Pm–Sm region join at ^{149,150}Sm (see Fig. 8). Indeed, the short half-lives of ^{149}Nd ($t_{1/2} = 2.21$ d) and ^{150}Pm ($t_{1/2} = 2.68$ h) leave ^{150}Sm virtually unbranched.

As anticipated in Section 2, ^{150}Sm is particularly suited to normalize the overall s-process predictions. We select ^{150}Sm because, besides being an unbranched s-only isotope, ^{150}Sm has very well-known MACS ($\sim$1 per cent uncertainty, σ[^{150}Sm(n, γ)] $= 422 \pm 4$ mbarn; KADoNiS) and solar abundance (5 per cent uncertainty, 0.265 ± 0.013 number of atoms per 10^6 Si atoms; Lodders et al. 2009).

Unlike ^{150}Sm, the ^{148}Sm abundance and, thus, the ^{148}Sm/^{150}Sm ratio are otherwise regulated by the branches at ^{147}Nd, ^{147}Pm and ^{148}Pm.

During the ^{13}C-pocket phase, the neutron density is not sufficient to bypass ^{148}Sm at the branching points ^{147}Nd ($t_{1/2} = 11$ d) and ^{148}Pm ($t_{1/2} = 5.37$ d) efficiently, whereas the branch at ^{147}Pm

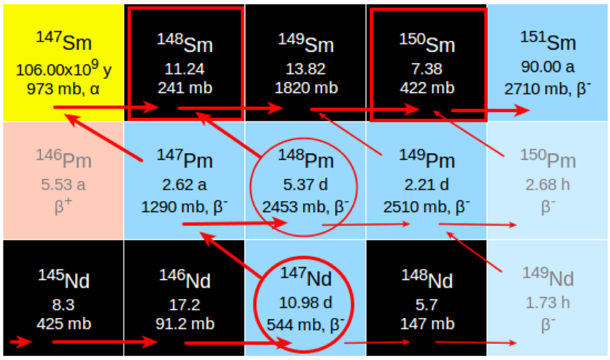

^{147}Sm 106.00x10^9 y 973 mb, α	^{148}Sm 11.24 241 mb	^{149}Sm 13.82 1820 mb	^{150}Sm 7.38 422 mb	^{151}Sm 90.00 a 2710 mb, β$^-$
^{146}Pm 5.53 a β$^+$	^{147}Pm 2.62 a 1290 mb, β$^-$	^{148}Pm 5.37 d 2453 mb, β$^-$	^{149}Pm 2.21 d 2510 mb, β$^-$	^{150}Pm 2.68 h β$^-$
^{145}Nd 8.3 425 mb	^{146}Nd 17.2 91.2 mb	^{147}Nd 10.98 d 544 mb, β$^-$	^{148}Nd 5.7 147 mb	^{149}Nd 1.73 h β$^-$

Figure 8. Schematic representation of the branches close to the s-only isotopes ^{148,150}Sm (red squares). Thick lines represent the s-process nucleosynthesis during the ^{13}C(α, n)^{16}O neutron irradiation, while thin lines correspond to the neutron capture channels open by the marginal activation of the ^{22}Ne(α, n)^{25}Mg reaction during TPs. Major branches at ^{147}Nd and ^{148}Pm, which regulate the s-contribution to ^{148}Sm, are highlighted by circles. All branches of the s-path join at ^{150}Sm, which is adopted to normalize the overall s-distribution. (This and the following figures are adapted from http://www.kadonis.org/.)

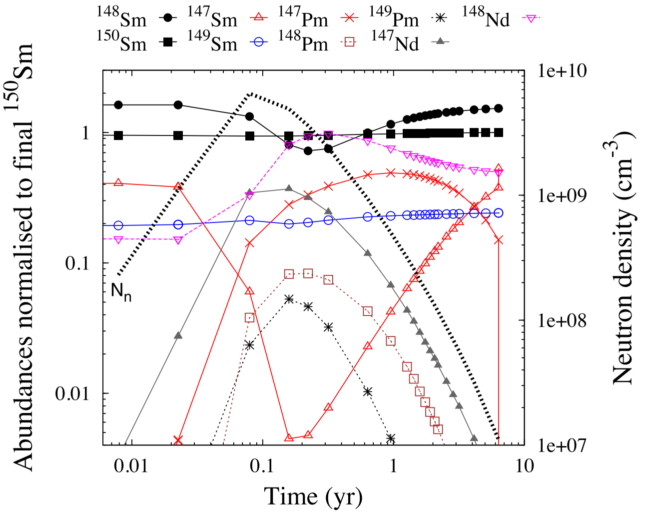

Figure 9. Temporal evolution of the neutron density and of the isotopic abundances of ^{147,148,149,150}Sm, ^{147,148}Nd and ^{147,148,149}Pm during the 15th He shell flash in an AGB star with 1.5 M$_\odot$ and half-solar metallicity. The abundance values are given as number fractions normalized to ^{150}Sm at the end of the He shell flash. The time-scale starts when the temperature at the bottom of the convective TP reaches $T_8 = 2.5$, which corresponds to the onset of the ^{22}Ne(α, n)^{25}Mg reaction. The initial abundances are those left from the previous ^{13}C-pocket phase.

($t_{1/2}$ = 2.62 yr) is partially activated (at $N_{\rm n} = 1 \times 10^7$ cm^{-3}, ~20 per cent of the *s*-path feeds ^{148}Pm, bypassing the long-lived ^{147}Sm).

On the other hand, the ^{147}Nd and ^{148}Pm neutron capture channels are activated during the ^{22}Ne(α, n)^{25}Mg irradiation. At the beginning of the TP, the neutron density strongly increases and ^{148}Sm is largely bypassed by the *s*-path. Under these conditions, the amount of ^{148}Sm produced during the previous ^{13}C-pocket phase is progressively depleted but starts to recover as the neutron density falls during the TP and is almost completely restored at the end of the TP (~94 per cent of the value produced at the end of the previous interpulse is re-established). In Fig. 9, we plot the temporal evolution of the neutron density and of the isotopic abundances of ^{147,148,149,150}Sm, $^{147,\,148}$Nd and ^{147,148,149}Pm during the 15th He shell flash for an AGB model with 1.5 M$_\odot$ and half-solar metallicity. The final ^{148}Sm abundance is predominantly determined by the freeze-out of the neutron supply, intuitively defined by the time when an isotopic abundance reaches 90 per cent of its final value (Cosner, Iben & Truran 1980; Arlandini et al. 1999). The abundance of a branched nucleus is frozen when the probability of further neutron captures (for the nearby unstable isotope) is marginal. Thus, the starting moment of the freeze-out depends on the MACS of the unstable isotope: the larger the MACS is, the later the freeze-out occurs.

The branch at ^{147}Pm ($t_{1/2} = 2.62$ yr, which following Takahashi & Yokoi 1987 is reduced to 1.2 yr at $T_8 = 3$) mainly affects the production of ^{147}Sm. The remaining ^{147}Pm abundance decays eventually into ^{147}Sm at the end of the TP.

The main component reproduces the solar abundance of ^{148}Sm (+5 per cent with respect to solar), in agreement within the solar uncertainty.

As for ^{150}Sm, also the MACS of ^{148}Sm is accurately known (241 ± 2 mbarn at 30 keV, KADoNiS; <1 per cent).

While the short half-lives of ^{147}Nd and ^{148}Pm are prohibitive for measuring their (n, γ) cross-sections with present techniques, the MACS of ^{147}Pm could be successfully determined via the activation method (709 ± 100 mbarn, 14 per cent; Reifarth et al. 2003; KADoNiS). Uncertainties of ~17 per cent have been estimated for the calculated MACS values of ^{147}Nd and ^{148}Pm (at 30 keV, σ[^{147}Nd(n, γ)] = 544 ± 90 mb, KADoNiS; σ[^{148}Pm(n, γ)] = 1014 ± 175 mbarn; Reifarth et al. 2003). The MACS uncertainties of the branch point isotopes ^{147}Nd, ^{147}Pm and ^{148}Pm have small effects on ^{148}Sm (<4 per cent in total).

Although ^{13}C(α, n)^{16}O is the major source of neutrons in low-mass AGB stars, the ^{148,150}Sm *s*-abundances are slightly influenced by the efficiency of the ^{22}Ne(α, n)^{25}Mg reaction: the *s*-production of ^{150}Sm increases by 4 per cent by including the recommended ^{22}Ne(α, n)^{25}Mg rate, and rises up to +12.5 per cent with Test A, while the relative contribution ^{148}Sm/^{150}Sm shows up to ~4 per cent variations (see Table 3). This variation reflects a more (or less) efficient *s*-process contribution during the TPs neutron burst independently of any branch, and affects the entire *s*-process distribution. On the other hand, the ^{22}Ne(α, n)^{25}Mg neutron source is crucial for regulating the ^{148,150}Sm abundances: the solar ^{148}Sm/^{150}Sm ratio would be overestimated by ~16 per cent by excluding its additional neutron irradiation (see column 5 of Table 3).

5.1.2 Additional unbranched isotopes

Besides ^{150}Sm (Section 5.1.1), ^{100}Ru, ^{104}Pd, ^{110}Cd, ^{116}Sn, ^{124}Te, ^{160}Dy, and ^{198}Hg are noteworthy *s*-only isotopes essentially unaffected by branches, and therefore also important for characterizing the entire *s*-process distribution.

At TP temperatures, the β-decay half-lives of their potential branch point isotopes are of the order of a couple of days, so that their decay rates clearly dominate over the respective neutron capture rates (compare e.g. the stellar half-lives of ^{99}Mo, ^{103}Ru, ^{110}Ag, ^{115}Cd, ^{122}Sb, ^{160}Tb, and ^{198}Au; Takahashi & Yokoi 1987).

Accordingly, the variations of the *s*-contributions to ^{100}Ru, ^{104}Pd, and ^{110}Cd in Fig. 6 include the cumulative effect of the normalization to ^{150}Sm (Section 5.1.1). The most well-known isotopes

Table 3. The *s*-production factors of ^{148}Sm and ^{150}Sm and their relative ratio (which corresponds to the *s*-contribution to solar ^{148}Sm) for different choices of the ^{22}Ne(α, n)^{25}Mg rate.

s-production factors	Recomm. ^{22}Ne(α, n)^{25}Mg rate (^{a})	TEST A Recomm. ^{22}Ne(α, n) × 4	TEST B Recomm. ^{22}Ne(α, n) × 0.9	[^{22}Ne(α, n)^{25}Mg] = 0 (^{b})
^{148}Sm	1194.1	1286.9 (+7.8 per cent)	1195.4 (<1 per cent)	1258.5 (+5.4 per cent)
^{150}Sm	1133.9	1275.5 (+12.5 per cent)	1128.4 (<1 per cent)	1088.4 (−4 per cent)
^{148}Sm/^{150}Sm (in per cent)	1.05	1.01 (−4 per cent)	1.06 (+1 per cent)	1.156 (+10.1 per cent)

Notes. (^{a}) Results obtained with our adopted ^{22}Ne(α, n)^{25}Mg rate (the same as Fig. 5).
(^{b}) Results with the contribution of the ^{13}C(α, n)^{16}O neutron source alone.

are ^{110}Cd, ^{124}Te, and ^{150}Sm, which have 5–7 per cent solar uncertainty and MACS values are known at ∼1 per cent. Less accurate MACS data with uncertainties of 6 and 10 per cent are affecting the *s*-prediction of ^{100}Ru and ^{104}Pd, although their solar abundances are well determined.

Utsunomiya et al. (2013) have indirectly determined the ^{99}Mo MACS via the inverse (γ, n) reaction. Although their estimated value at 30 keV is significantly larger than the theoretical MACS recommended by KADoNiS (410 instead of 240 mb), the effect on the *s*-prediction for ^{100}Ru is only ∼1 per cent.

The *s*-abundances of ^{116}Sn and ^{124}Te are reproduced in agreement within the solar uncertainties (15 and 7 per cent, respectively; Lodders et al. 2009).

The *s*-abundances of ^{160}Dy and ^{198}Hg are difficult to determine as discussed in detail in Appendix B (Supporting Information).

About 10 per cent of solar ^{160}Dy is missing. This dearth may be reconciled within the uncertainties: although the (n, γ) cross-section of ^{160}Dy is very well determined in laboratory (σ[^{160}Dy(n, γ)] = 890 ± 12 mbarn at 30 keV, 1.4 per cent; KADoNiS), the MACS remains rather uncertain in this case due to a significant stellar enhancement factor (SEF = 1.12 at 30 keV; KADoNiS). This correction may provide the 10 per cent missing *s*-process contribution to solar ^{160}Dy. The solar abundance of Dy is instead well determined (5 per cent by Lodders et al. 2009).

The *s*-contribution to solar ^{198}Hg is very uncertain, mainly because Hg is a volatile element, and its solar abundance is affected by 20 per cent uncertainty (Lodders et al. 2009). An additional 8.7 per cent uncertainty derives from the ^{198}Hg MACS (173 ± 15 mbarn; dated back to Beer & Macklin 1985; KADoNiS).

Note that the large uncertainties associated with the ^{116}Sn and ^{198}Hg *s*-contributions derive from the poorly known Sn and Hg solar abundances.

5.2 The *s*-only isotopes sensitive to the neutron density

In this section, we analyse the *s*-contribution to ^{96}Mo, which is influenced by the branch at ^{95}Zr. This branching depends only on the neutron density because the β-decay rate of ^{95}Zr remains constant at the relevant *s*-process temperatures.

The *s*-only isotopes ^{170}Yb, ^{142}Nd, ^{186}Os and ^{192}Pt belong to this class of branchings as well. Although the half-lives of their related branch point nuclides exhibit a marginal sensitivity to stellar temperature, the respective MACS uncertainties still dominate over the temperature effects.

5.2.1 The s-only isotope ^{96}Mo (the branch at ^{95}Zr)

In this atomic mass region, the long-lived ^{93}Zr behaves as a stable isotope during the main *s*-process ($t_{1/2}$ = 1.5 × 10^6 yr; Fig. 10). The *s*-path directly feeds ^{94}Zr, bypassing ^{92,94}Mo (two *p*-only isotopes, mainly destroyed during AGB nucleosynthesis). The radioactive decay of ^{93}Zr into ^{93}Nb occurs after the end of the TP-AGB phase, when the *s*-process nucleosynthesis stops (e.g. Wallerstein & Dominy 1988). This decay produces a decrease of the relative [Zr/Nb] ratio. Similarly to the discovery of Tc in the spectrum of an AGB star of spectral type S (Merrill 1952; Lambert et al. 1995), the [Zr/Nb] ratio supplies spectroscopic information about the synthesis of heavy elements in evolved stars (see e.g. Ivans et al. 2005; Kashiv et al. 2010).

The abundance of ^{96}Mo is dominated by the branch point at ^{95}Zr ($t_{1/2}$ = 64.03 d). At the low neutron density reached during the ^{13}C-pocket phase (∼10^7 cm^{-3}), most of the *s*-flow proceeds towards ^{95,96}Mo, but moderate neutron captures on ^{95}Zr are allowed at the peak neutron density achieved during TPs ($N_\mathrm{n} \gtrsim 1 \times 10^9$ cm^{-3}; $f_\mathrm{n} \gtrsim 0.1$). Under these conditions, the *s*-path feeds the neutron-rich ^{96}Zr (about 3 per cent of solar Zr), and ^{95,96}Mo are partially bypassed.

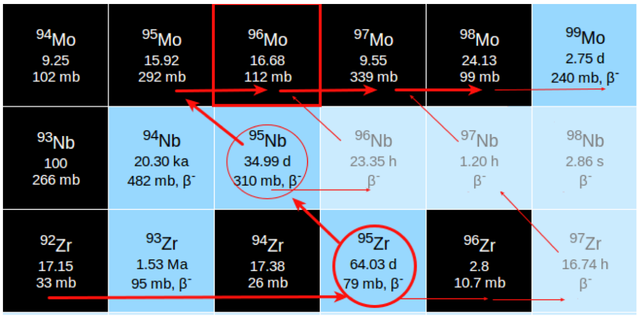

Figure 10. The same as Fig. 8, but for the *s*-path region close to the *s*-only isotope ^{96}Mo (red rectangle). While ^{93}Zr is practically stable on the time-scale of the *s*-process, ^{95}Zr acts as the main branching point.

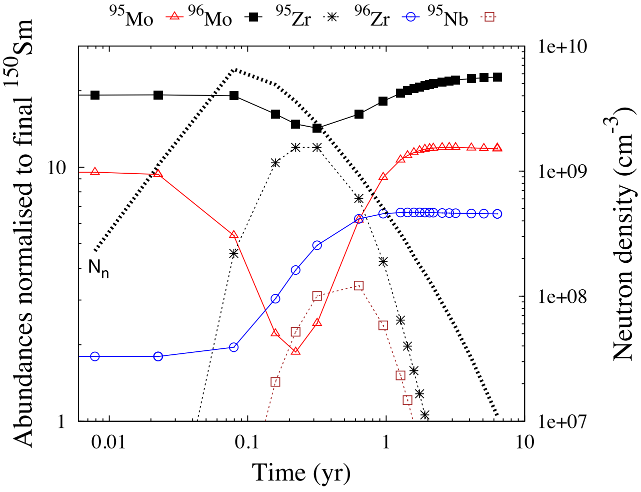

Figure 11. The same as Fig. 9, but for the isotopic abundances of ^{95,96}Mo, ^{95,96}Zr and ^{95}Nb.

Fig. 11 shows the temporal evolution of the neutron density and of the isotopic abundances of ^{95,96}Mo, ^{95,96}Zr and ^{95}Nb during the 15th He shell flash in an AGB star with 1.5 M$_\odot$ and half-solar metallicity. At the peak neutron density ^{96}Mo is depleted, but as soon as the neutron density decreases, ^{96}Mo starts rising again to exceed the values at the end of the previous interpulse by 18 per cent.

While ^{96,97}Mo and ^{96}Zr are only influenced by the branch at ^{95}Zr, ^{95}Mo is mostly bypassed by the *s*-path owing to the branch at ^{95}Nb ($t_{1/2}$ = 34.99 d; $N_\mathrm{n} > 4 \times 10^9$ cm^{-3}, $f_\mathrm{n} > 0.5$).

The ^{95}Zr MACS is largely uncertain, and discrepant values are found in literature: KADoNiS recommends the value estimated by Bao et al. (2000, 79 ± 12 mb at 30 keV), with a rather small uncertainty (15 per cent), whereas Toukan & Käppeler (1990) estimated a value of 50 mb at kT = 30 keV. Recently, Lugaro et al. (2014b) provided a value that was 50 per cent lower than that of Toukan & Käppeler (1990) and about three times lower than in KADoNiS. Accordingly, the MACS of ^{95}Zr is still affected by an uncertainty of about a factor of 2.

In our AGB models, a value close to that suggested by Toukan & Käppeler (1990) was adopted so far for the ^{95}Zr MACS.

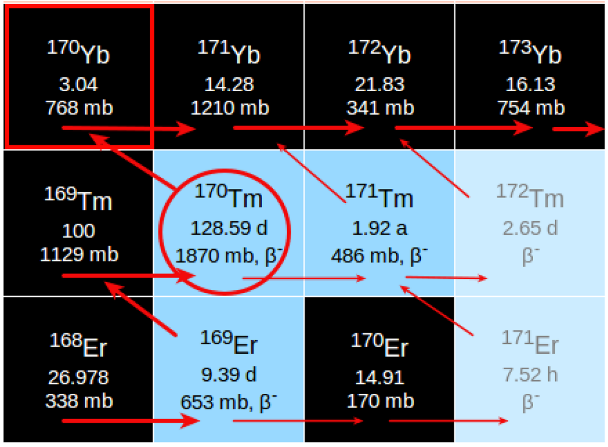

Figure 12. The same as Fig. 8, but for the *s*-path close to the *s*-only isotope ^{170}Yb (red rectangle). The branch at ^{170}Tm (marked by the circle) is activated mainly during TPs.

In Table 4, we list the *s*-contributions to isotopes from ^{94}Zr to ^{98}Mo. By including the old ^{22}Ne(α, n)^{25}Mg rate, the *s*-contribution to solar ^{96}Mo was overestimated by +4 per cent (column 2; which include our guess on the ^{95}Zr MACS); this value slightly increases to +8 per cent by adopting the new theoretical ^{95}Zr MACS evaluated by Lugaro et al. (2014b, column 3).

Updated *s*-predictions (which include the recommended ^{22}Ne(α, n)^{25}Mg rate and the ^{95}Zr MACS by Lugaro et al. 2014b) reproduce 99 per cent of solar ^{96}Mo. Note that the solar ^{96}Mo is largely overestimated (+20 per cent) with increasing the recommended ^{22}Ne(α, n)^{25}Mg rate by factor of 4 (Test A). This exceeds the solar Mo uncertainty (10 per cent; Lodders et al. 2009) and the ^{96}Mo MACS uncertainty (7 per cent; 112 ± 8 mbarn at 30 keV; KADoNiS), which dated back to an earlier measurement by Winters & Macklin (1987).

Major changes are shown by ^{96}Zr. Although ^{96}Zr is a neutron-rich isotope, it receives an important *s*-contribution during the ^{22}Ne(α, n)^{25}Mg neutron burst in AGB stars: once built-up by the activation of the branch at ^{95}Zr, ^{96}Zr is only marginally destroyed by neutron captures owing to its small MACS (10.3 ± 0.5 mb at 30 keV; Tagliente et al. 2011b). Starting from Arlandini et al. (1999), the main component was known to produce about half of the solar ^{96}Zr. Present calculations obtained with the recommended ^{22}Ne(α, n)^{25}Mg rate reduce this contribution from 50 to 14 per cent. This value is extremely sensible to the ^{22}Ne(α, n)^{25}Mg rate: Test A yields an increase by a factor 6 (87 per cent). Moreover, a factor of 2 uncertainty is still associated with the theoretical ^{95}Zr MACS.

We remind that ^{96}Zr is a well-known indicator of the initial AGB mass. An additional *s*-contribution to ^{96}Zr comes from IMS AGB stars (Travaglio et al. 2004). Indeed, although IMS stars marginally produce heavy *s*-isotopes, the strong neutron density reached during TPs ($N_{\rm n} \sim 10^{11}$ cm^{-3}) may significantly increase the abundance of ^{96}Zr (see Appendix C, Supporting Information).

5.2.2 *The* s*-only isotope* ^{170}*Yb (the branches at* ^{169}*Er and* ^{170}*Tm)*

The abundance of ^{170}Yb is regulated by the branches at ^{170}Tm (see Fig. 12) and to a minor extent at ^{169}Er (whose terrestrial half-life $t_{1/2} = 9.4$ d decreases to $t_{1/2} \sim 7.5$ d at $T_8 = 3$; Takahashi & Yokoi 1987). Neutron captures on ^{169}Er are only relevant at high neutron densities ($N_{\rm n} \gtrsim 3 \times 10^9$ cm^{-3}; $f_{\rm n} \gtrsim 0.3$).

The *s*-contribution to ^{170}Yb is essentially determined by the branch at ^{170}Tm due to its comparably long half-life ($t_{1/2}(\beta^-) = 128.59$ d, almost independent of temperature. ^{170}Yb is efficiently bypassed ($f_{\rm n} \gtrsim 0.5$) by the *s*-process flow for neutron densities larger than about 1.3×10^8 cm^{-3} when neutron captures prevail over β decays. Fig. 13 shows the temporal evolution of the neutron density and of the isotopic abundances of ^{170,171}Yb, ^{169,170}Tm and ^{168,169,170}Er during the 15th He shell flash in a 1.5 M$_\odot$ model and half-solar metallicity. ^{170}Yb is strongly depleted during the peak neutron density, when both ^{169}Er and ^{170}Tm branches are activated and the *s*-path proceeds mainly via ^{171}Tm ($t_{1/2} = 1.92$ yr), thus bypassing ^{171}Yb as well. Most of ^{170}Yb is restored as the neutron density decreases (~74 per cent of the ^{170}Yb abundance produced during the previous ^{13}C pocket is re-established). Note that the ^{170}Tm β^+-decay channel to ^{170}Er is negligible (Takahashi & Yokoi 1987).

The main component reproduces 99 per cent of solar ^{170}Yb. About 10 per cent of solar ^{170}Yb is missing with increasing the recommended ^{22}Ne(α, n)^{25}Mg rate by a factor of 4. The MACS of ^{170}Yb is very well determined with less than 1 per cent uncertainty (768 ± 7 at 30 keV; KADoNiS). The major uncertainty that affects the

Table 4. Old solar main component isotopic percentage contributions from ^{94}Zr to ^{98}Mo (column 2; computed with our estimated ^{95}Zr MACS, close to that recommended by Toukan & Käppeler 1990; 'OLD'), compared with our previous calculations (column 3; which include the ^{95}Zr MACS by Lugaro et al. 2014b; 'L14') and with *s*-predictions obtained by assuming the ^{95}Zr MACS by KADoNiS (column 4; 'KAD'). In column 5, we list the updated main component obtained with the recommended ^{22}Ne(α, n)^{25}Mg rate (Fig. 5). In column 6, we provide the results of Test A in Section 4.1, in which we multiplied by a factor of 4 the recommended ^{22}Ne(α, n)^{25}Mg rate. Only variations larger than 5 per cent are given in brackets.

	Tests of the ^{95}Zr(n, γ)^{86}Kr MACS				
Isotope	OLD	L14	KAD	L14	L14
		[Old ^{22}Ne(α,n)]		[Recomm. ^{22}Ne(α,n)]	[Recomm. ^{22}Ne(α,n) × 4]
^{94}Zr	105.4	105.5	105.4	107.4	104.2
^{96}Zr	50.0 (1.40)	35.6	84.3 (2.37)	14.3 (0.40)	87.4 (2.46)
^{93}Nb	71.5	71.5	71.6	69.2	73.5
^{95}Mo	60.8	62.8	56.2 (0.90)	60.4	61.7
^{96}Mo	104.0	108.0	94.8 (0.88)	99.2 (0.92)	120.5 (1.12)
^{97}Mo	55.0	56.3	51.9 (0.92)	53.4	65.3 (1.16)
^{98}Mo	69.6	70.3	67.8	74.7 (1.06)	71.0

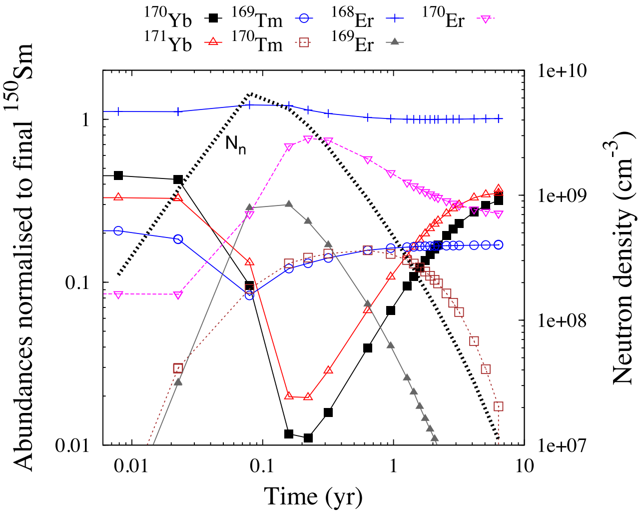

Figure 13. The same as Fig. 9, but for the isotopic abundances of ^{170,171}Yb, ^{169,170}Tm and ^{168,169,170}Er.

abundance of ^{170}Yb is related to its SEF (∼1.08 at $kT = 23$ keV; KADoNiS).

Other uncertainties derive from the theoretical MACS of ^{170}Tm (1870 ± 330 at 30 keV; 17.6 per cent), which produces up to 6 per cent variation on the ^{170}Yb *s*-predictions, and from the ^{170}Tm β^--decay rate, for which Goriely (1999) estimated up to a factor of 1.7 uncertainty at $T_8 = 3$, affecting the *s*-contribution to ^{170}Yb by ∼4 per cent.

5.2.3 *Additional branches sensitive to the neutron density*

Besides ^{96}Mo and ^{170}Yb, we underline ^{142}Nd, ^{186}Os and ^{192}Pt among the isotopes mainly sensitive to the ^{22}Ne(α, n)^{25}Mg neutron burst.

Similar to the branch at ^{95}Zr, the β-decay rates of ^{85}Kr and ^{86}Rb are constant at stellar temperature, and the *s*-contributions to ^{86,87}Sr are mainly sensitive to the neutron density reached during the ^{22}Ne(α, n)^{25}Mg irradiation. The effect of the above branchings on the abundances of ^{86,87}Sr as well as on the neutron-magic nuclei ^{86}Kr and ^{87}Rb during the ^{13}C-pocket and TP phases are discussed in Appendix B (Supporting Information).

The solar abundance of the neutron-magic isotope ^{142}Nd is affected by the branches at ^{141}Ce and ^{142}Pr (partially open during TP), and decreases by ∼15 per cent with increasing the recommended ^{22}Ne(α, n)^{25}Mg rate by a factor of 4.

While the solar abundances of ^{96}Mo, ^{170}Yb and ^{142}Nd are plausibly represented by the main component, the interpretation of solar ^{186}Os and ^{192}Pt is more problematic.

The studies carried out by Mosconi et al. (2010) and Fujii et al. (2010) have substantially increased the accuracy of the ^{186}Os MACS (4.1 per cent). The *s*-abundance of ^{186}Os is mainly influenced by the branch at ^{185}W, while smaller variations are produced by the branch at ^{186}Re (β decay rather constant at stellar temperatures). Although the half-life of ^{185}W is slightly sensitive to temperature and electron density ($t_{1/2} = 75.10$ d decreases to 50 d at $T_8 = 3$; Takahashi & Yokoi 1987), the *s*-abundance of ^{186}Os is dominated by the uncertainty of the theoretical MACS of ^{185}W. The present ^{185}W(n, γ) cross-section overestimates the solar ^{186}Os abundance by 20–30 per cent, hardly to be reconciled with the 8 per cent uncertainty of the solar abundance (Lodders et al. 2009). The accuracy of the ^{185}W MACS recommended by KADoNiS (9 per cent) could be largely underestimated (see Rauscher 2014), being based on an average among inverse (γ, n) reactions (Sonnabend et al. 2003; Mohr et al. 2004; Shizuma et al. 2005). In order to reproduce the solar abundance with our AGB models, we adopt a MACS for ^{185}W which is about 80 per cent higher than recommended in KADoNiS.

Present calculations underestimate the solar ^{192}Pt abundance by ∼20 per cent. The abundance of ^{192}Pt is mainly determined by the branch at ^{192}Ir. Similar to ^{186}Os, the *s*-contribution of ^{192}Pt is also dominated by the uncertainty of the neutron capture channel rather than by the β-decay branch (slight reduction of the half-life of ^{192}Ir from 77.54 d to 55.33 d at $T_8 = 3$; Takahashi & Yokoi 1987). The MACS measurements on the Pt isotopes by Koehler & Guber (2013) included also a new calculation of the values for ^{192}Ir. The discrepancy is reduced by accounting of a 20 per cent uncertainty of the theoretical ^{192}Ir MACS, which increases the ^{192}Pt *s*-prediction to ∼85 per cent. However, a 15 per cent missing contribution scarcely agrees with the much improved accuracy of the ^{192}Pt MACS measured by Koehler & Guber (2013, 4 per cent), and with an 8 per cent solar uncertainty (Lodders et al. 2009). A more detailed theoretical analysis of the branch at ^{192}Ir would help to improve the ^{192}Pt *s*-prediction.

In Appendix B (Supporting Information), the uncertainties affecting the *s*-predictions of ^{142}Nd, ^{186}Os and ^{192}Pt are analysed in detail.

While the *s*-contribution of ^{192}Pt is marginally influenced by the ^{22}Ne(α, n)^{25}Mg uncertainty, the present *s*-contributions to solar ^{96}Mo and ^{170}Yb better agree with our newly evaluated ^{22}Ne(α, n)^{25}Mg rate. However, the MACS of ^{170}Yb is affected by a non-negligible SEF correction (1.15 at 30 keV; KADoNiS) although its neutron capture cross-section is well determined experimentally (see also Rauscher et al. 2011).

5.3 The *s*-only isotopes strongly sensitive to stellar temperature (and/or electron density) and neutron density

The β-decay rates of several unstable isotopes exhibit a strong dependence on temperature and electron density (Takahashi & Yokoi 1987). As anticipated in Section 5, the uncertainty affecting the stellar β-decay rate of a few branches may produce wide variations of the *s*-predictions.

The branches at issue are ^{134}Cs (affecting the *s*-contribution to solar ^{134}Ba), ^{151}Sm and ^{154}Eu (which influence the ^{152,154}Gd abundances), ^{176}Lu (making it an *s*-process thermometer rather than a cosmic clock) and ^{204}Tl (with consequences for the *s*-contribution of ^{204}Pb).

5.3.1 *The* s*-only pair ^{134,136}Ba (the branch at ^{134}Cs)*

The production of the two *s*-only isotopes ^{134,136}Ba occurs via both neutron irradiations, in the ^{13}C pocket and during TPs.

Most of solar ^{134}Ba is produced in the ^{13}C pocket, when the *s*-path proceeds via ^{132}Xe and ^{133}Cs directly to ^{134}Ba, because the low neutron density does not allow neutron captures on ^{133}Xe and ^{134}Cs (Fig. 14). In this way, the solar ^{134}Ba/^{136}Ba ratio would be overestimated by about a factor of 2. The additional ^{22}Ne(α, n)^{25}Mg neutron burst partially activated during TP is essential to regulate the ^{134,136}Ba predictions in order to reproduce the solar abundances. The main component is expected to reproduce the *s*-contribution of the *s*-only pair ^{134}Ba and ^{136}Ba so that ^{134}Ba:^{136}Ba = 1:1 within solar and nuclear uncertainties.

The dominant uncertainty affecting the ^{134}Ba/^{136}Ba ratio derives from the β^--decay rate of ^{134}Cs: the terrestrial half-life of ^{134}Cs

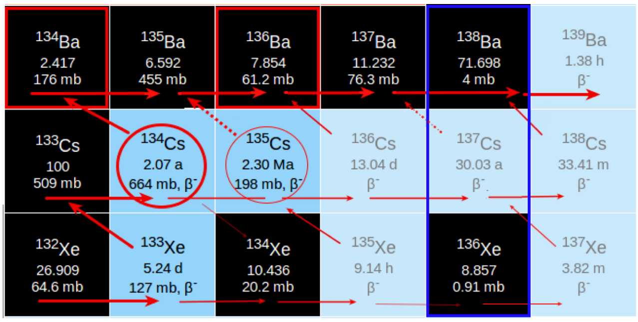

Figure 14. The same as Fig. 8, but for the *s*-path close to the *s*-only isotopes ^{134}Ba and ^{136}Ba (red squares). The main branch point occurs at ^{134}Cs. The electron-capture (EC) channel of ^{134}Cs is negligible. The long-lived ^{135}Cs can be considered almost stable during the *s*-process, and its radiogenic contribution to ^{135}Ba occurs after the TP-AGB phase (thick dashed arrow); the abundance of ^{137}Cs stored during TPs β^- decays to ^{137}Ba during interpulse periods (thin dashed arrow). The neutron-magic nuclei at $N = 82$ are indicated by a blue box.

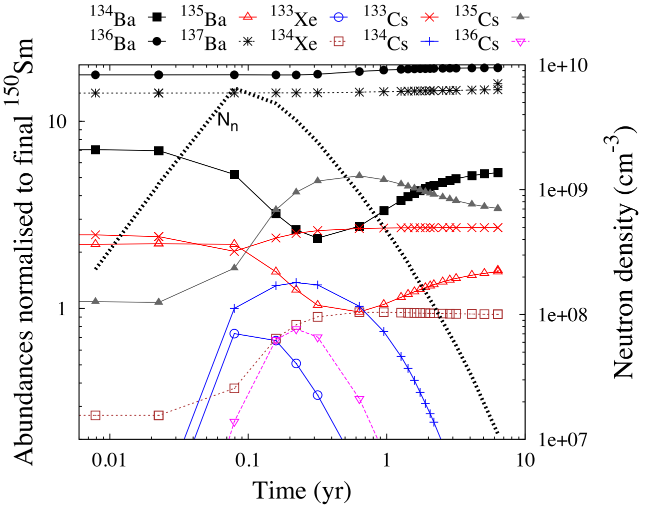

Figure 15. The same as Fig. 9, but for ^{134,135,136,137}Ba, ^{133,134}Xe and ^{133,134,135,136}Cs isotopic abundances.

($t_{1/2} = 2.07$ yr) is strongly reduced under stellar conditions (Takahashi & Yokoi 1987): it decreases by a factor of 3 at $T_8 = 1$ (0.67 yr) and by two orders of magnitude at $T_8 = 3$ (3.8 d). Note that $\lambda^-(^{134}\mathrm{Cs})$ does not change with electron (or mass) density.

In previous AGB models (see filled circles in Fig. 5), we have adopted a constant β^--decay rate for ^{134}Cs, which was based on a geometric average of the rates given by Takahashi & Yokoi (1987) at different temperatures over the convective pulse ($\lambda^-(^{134}\mathrm{Cs}) = 1.6 \times 10^{-7}$ s^{-1}, $t_{1/2} = 50$ d; see Bisterzo et al. 2011; Liu et al. 2014). This value reproduces the solar ^{134}Ba/^{136}Ba ratio, and the predicted *s*-contributions exceed the solar abundances of ^{134}Ba and ^{136}Ba by only 6 and 9 per cent, respectively, well within the uncertainties quoted for the solar abundances (6 per cent for Ba, 5 per cent for Sm; Lodders et al. 2009) and for the MACS values of barium (3.2 per cent at 30 keV; KADoNiS).

The strong temperature dependence of the half-life of ^{134}Cs is now considered by an improved treatment of the β-decay rate as a function of the temperature gradient within the TPs. The maximum temperature reached by a given AGB model at the bottom of the convective intershell rises from pulse to pulse. The convective TP itself is characterized by a very large gradient in temperature and density, which decreases from $T_8 \sim 3$ and $\rho = 2 \times 10^4$ g cm^{-3} at the bottom of the advanced TP to $T_8 \sim 0.1$ and $\rho = 10$ g cm^{-3} in the top layers. Under these conditions, the ^{134}Cs half-life varies from 2 yr in the top layers of the convective TP (where no neutrons are available) down to 3.8 d in the region of highest neutron density at the bottom. Accordingly, the production of ^{134}Cs depends strongly on the locus inside the TP: for $T_8 \sim 3$, one finds $t_{1/2} = 3.8$ d, and at $N_\mathrm{n} \sim 4 \times 10^9$ cm^{-3} only ~25 per cent of the *s*-flow bypasses ^{134}Ba. Slightly further outward, at $T_8 \sim 2.7$, neutrons are still produced via ^{22}Ne(α, n)^{25}Mg, but the half-life of ^{134}Cs has increased to 50 d: under these conditions, neutron captures dominate over β decays starting from $N_\mathrm{n} \sim 10^9$ cm^{-3} ($f_\mathrm{n} \sim 0.5$), and ^{134}Ba is more efficiently bypassed.

We have interpolated (with a cubic-spline method) the β^--decay rates given by Takahashi & Yokoi (1987) as a function of the stellar temperature in the range from $T_8 = 0.5$ to 5. The adopted rate results very close to that recommended by NETGEN.[7] ^{134}Cs is freshly produced in the thin bottom layers of the TP, but even in this hot environment ^{134}Cs has half-life of a few days, much larger than the turnover time, so that it is quickly brought to the outer and cooler layers of the TPs. Here, the ^{134}Cs half-life increases up to 2 yr, but the lack of neutrons does not allow further neutron captures and it decays into ^{134}Ba. Because a small amount of ^{134}Cs is converted to ^{135}Cs during the peak neutron density at the bottom of the TPs, ^{134}Ba is temporarily reduced (by ~30 per cent). The initial amount of ^{134}Ba is almost fully re-established as soon as the neutron density decreases. Consequently, almost the entire *s*-flow is directed towards ^{134}Ba, resulting in a large overestimation of solar ^{134}Ba (+30 per cent).

This problem with the branching at ^{134}Cs can be somewhat relaxed if one considers the uncertainty in the temperature-dependent half-life. Goriely (1999) estimated a possible decrease of the decay rate by a factor of ~3 at $T_8 = 2$–3. Assuming twice that change as 2σ-uncertainty would reduce the overestimation of the solar ^{134}Ba (see *filled diamond* in Fig. 5). In this case, ^{134}Ba is largely depleted at the beginning of the advanced TPs (see e.g. Fig. 15, which shows the temporal evolution of the isotopic abundances during the 15th TP in a 1.5 M$_\odot$ model at half-solar metallicity). As the neutron density decreases, the β^--decay channel is favoured and the ^{134}Ba abundance is increasing again ($N_\mathrm{n} \lesssim 2 \times 10^8$ cm^{-3}; $f_\mathrm{n} \leq 0.1$). About 76 per cent of ^{134}Ba produced during the previous ^{13}C pocket is restored at the tail of the neutron density. The resulting *s*-contributions to ^{134}Ba and ^{136}Ba exceed the solar abundances by +12 and +9 per cent, respectively. This may suggest that the stellar ^{134}Cs β^-decay rate by Takahashi & Yokoi (1987) has been overestimated. Further investigations on this topic are advised.

An additional important effect concerning the *s*-predictions for the Ba isotopes derives from the ^{22}Ne(α, n)^{25}Mg rate. The above *s*-contributions to ^{134}Ba and ^{136}Ba may be reduced to +4 and +2 per cent with increasing the recommended ^{22}Ne(α, n)^{25}Mg rate by a factor of 4 (Test A).

A marginal impact on the ^{134,136}Ba *s*-predictions derives from the branches at ^{133}Xe and ^{135,136}Cs. The short half-life of ^{133}Xe ($t_{1/2} = 5.24$ d) does not allow efficient neutron captures (less than 2 per cent of the *s*-flow feeds ^{134}Xe).

Although the terrestrial half-life of the long-lived ^{135}Cs ($t_{1/2} = 2.3$ Myr) is reduced by four orders of magnitude at $T_8 = 3$ (e.g. $t_{1/2} = 267$ yr at $\rho = 3000$ g cm^{-3}; Takahashi & Yokoi 1987), it is practically stable compared to the 6 yr time-scale of the ^{22}Ne(α,

---

[7] Website: http://www.astro.ulb.ac.be/Netgen.

n)^{25}Mg irradiation with a TP. Therefore, once the *s*-flow feeds ^{135}Cs, it proceeds towards ^{136}Cs, and ^{135}Ba may be easily bypassed (see Fig. 15). The abundance of the long-lived ^{135}Cs stored during TPs β^- decays into ^{135}Ba at the end of the TP-AGB phase.

The *s*-flow at ^{136}Cs ($t_{1/2}$ = 13.04 d) continues mainly via β^- decay to ^{136}Ba, where the two *s*-branches formed at ^{134}Cs join again. Accordingly, the *s*-contribution to ^{136}Ba keeps increasing during the entire ^{22}Ne(α, n)^{25}Mg irradiation, thus enhancing the abundance from the previous ^{13}C pocket by +10 per cent.

The ^{134}Cs MACS has been estimated semi-empirically by Patronis et al. (2004), who provide a rather small uncertainty of 9 per cent (KADoNiS), resulting in a ~2.5 per cent variation of the ^{134}Ba abundance. The uncertainties of the theoretical MACS values of ^{133}Xe (KADoNiS) and ^{136,137}Cs (Patronis et al. 2004) are presently estimated between 30 and 50 per cent, but have almost no impact (<2 per cent) on ^{134,136}Ba.

5.3.2 Additional branches strongly sensitive to stellar temperature (and/or electron density) and neutron density

A few branches behave as thermometers of the *s*-process in AGB stars because their β-decay rates deeply rise (or drop) with the large temperature and electron density gradients that characterize a convective TP (Takahashi & Yokoi 1987). In a few cases, this β-decay behaviour is responsible for crucial uncertainties.

Similar to the way ^{134}Cs affects the *s*-contribution to ^{134}Ba, the decay rates of ^{151}Sm and ^{154}Eu depend strongly on temperature and electron density during TPs with corresponding consequences for the *s*-abundances of ^{152}Gd and ^{154}Gd, respectively.

The *s*-predictions to ^{152,154}Gd have been improved by including in AGB models an appropriate treatment of the nearby β-decay rates over the full convective TPs (see *filled diamonds* in Fig. 5): about 85 and 92 per cent of solar ^{152}Gd and ^{154}Gd are produced by AGB stars. According to Goriely (1999), both rates may vary up to a factor of 3 at $T_8 = 3$. This would produce an extreme impact on the ^{152}Gd *s*-prediction (up to a factor of 2), and up to 10–15 per cent variations of the ^{154}Gd *s*-contribution. The dominant effect of the ^{151}Sm half-life prevents the *s*-contribution to solar ^{152}Gd from being accurately assessed. Additional uncertainties may derive from the ^{151}Sm and ^{154}Eu MACS (see Rauscher et al. 2011).

Certainly, the *s*-predictions of the above isotopes are largely influenced by the uncertainties of the ^{22}Ne(α, n)^{25}Mg rate. A detailed analysis of these aspects is given in Appendix B (Supporting Information).

Two other isotopes are worth mentioning, where the AGB contributions depend strongly on temperature: the long-lived ^{176}Lu (more properly classified as an *s*-process thermometer rather than a cosmic clock), and ^{204}Tl (which regulates the *s*-contribution of solar ^{204}Pb).

At present, the discrepancy between experimental data and the astrophysical treatment of the branch at ^{176}Lu remains to be solved (Heil et al. 2008c; Mohr et al. 2009; Cristallo et al. 2010). The solution may be found in the nuclear coupling scheme between thermally populated levels in ^{176}Lu (Gintautas et al. 2009; Dracoulis et al. 2010; Gosselin, Morel & Mohr 2010). Besides the branch at ^{176}Lu, the ^{22}Ne(α, n)^{25}Mg rate and the SEF estimate of the ^{176}Hf MACS are directly influencing the predicted ^{176}Lu/^{176}Hf ratio.

Although the MACS of ^{204}Pb is accurately known (3 per cent), the present ^{204}Pb *s*-prediction is jeopardized by the uncertainty of the theoretical ^{204}Tl neutron capture cross-section and by the evaluation of its stellar β^--decay rate (~10 per cent variations). An additional 10 per cent uncertainty from the solar Pb abundance (Lodders et al. 2009) has to be considered as well.

The impact of the present uncertainties is discussed in Appendix B (Supporting Information).

5.4 The *s*-only isotopes mainly sensitive to stellar temperature (and electron density)

The branches at issue are ^{179}Hf (responsible for the *s*-contribution to ^{180}Ta^m; see e.g. Käppeler et al. 2004; Wisshak et al. 2004), ^{164}Dy (which produced about half of solar amount of the proton-rich isotope ^{164}Er; Jaag & Käppeler 1996) and ^{128}I (which regulates the *s*-production to ^{128}Xe; Reifarth et al. 2004).

Because of their low sensitivity to the neutron density, the branches at ^{180}Ta^m and ^{128}I have provided information on the convective mixing time-scale. However, the large uncertainties of the β-decay rates of the respective branch point nuclei have led to problems in the interpretation of the branchings towards ^{164}Er and ^{180}Ta^m.

5.4.1 The s*-contribution to ^{180}Ta^m (the branches at ^{179}Hf, ^{179}Ta and ^{180}Hf)*

In the Solar system, ^{180}Ta occurs only in its stable isomer ($t_{1/2}$ > 10^{15} yr). ^{180}Ta^m is the rarest stable isomer in nature and constitutes 0.012 per cent of solar Ta. The ground state of ^{180}Ta is unstable and decays with a half-life of 8.15 h by β^- and β^+ emission to ^{180}W and ^{180}Hf, respectively.

The origin of ^{180}Ta^m has been a challenge for years. Being proton-rich, the expected contributions from p(γ)- and νp-processes have been largely investigated (e.g. Rayet et al. 1995; Rauscher et al. 2002; Heger et al. 2005). As illustrated in Fig. 16, the *s*-flow is bypassing ^{180}Ta^m because ^{179,180}Hf are stable during the ^{13}C(α, n)^{16}O irradiation. At the higher temperatures during TPs, however, higher lying nuclear states in ^{179}Hf and ^{180}Hf are thermally populated, opening two branches towards ^{180}Ta^m: (i) via β^- decay of the thermally populated ^{179}Hf state at 214 keV, which β^- decays to ^{179}Ta and produces ^{180}Ta^m via neutron captures, and (ii) via the ^{179}Hf

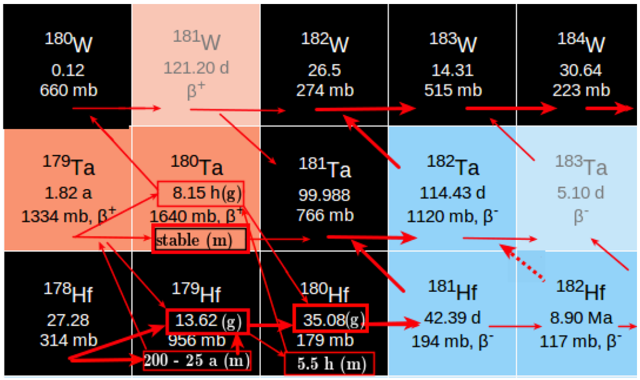

Figure 16. The same as Fig. 8, but for the *s*-path close to ^{180}Ta^m. During the ^{13}C(α, n)^{16}O neutron irradiation, ^{179}Hf is stable and the *s*-path follows the thick red lines; during ^{22}Ne(α, n)^{25}Mg neutron burst (thin red lines), the isomeric state of ^{179}Hf becomes unstable (with half-life strongly temperature dependent; Takahashi & Yokoi 1987), allowing the branch of the *s*-flow towards ^{179}Ta, and the stable ^{180}Ta^m. The long-lived ^{182}Hf ($t_{1/2}$ = 8.9 Myr) can be considered almost stable during the *s*-process, and its radiogenic contribution to ^{182}Ta occurs after the TP-AGB phase (red dashed thick line).

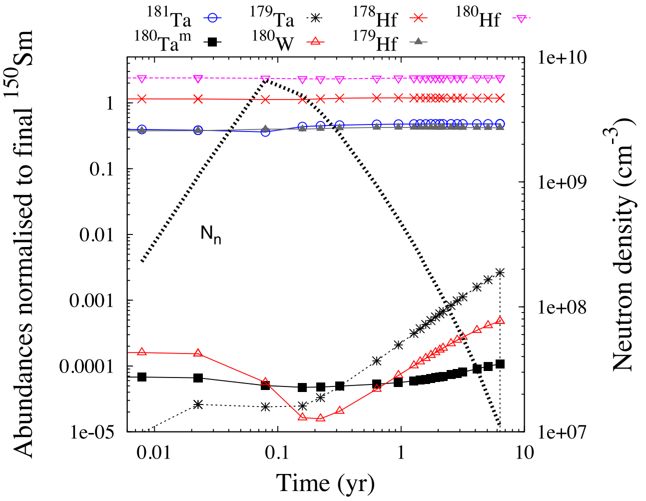

Figure 17. The same as Fig. 9, but for the isotopic abundances of ^{180}Ta^m, ^{179,181}Ta,^{180}W and ^{178,179,180}Hf.

partial neutron capture cross-section towards the weakly populated ^{180}Hf isomer, which β^- decays quickly to ^{180}Ta^m.

Several studies have been dedicated to the *s*-process nucleosynthesis of ^{180}Ta^m (e.g. Németh, Käppeler & Reffo 1992; Käppeler et al. 2004; Wisshak et al. 2004, 2006c; Mohr, Käppeler & Gallino 2007).

Briefly, about half of the *s*-contribution to ^{180}Ta^m is produced via the branch at ^{179}Hf^m. At $T_8 = 3$, the ^{179}Hf half-life becomes sensitive to temperature and electron density (e.g. $t_{1/2}$ from 85 to 25 yr; Takahashi & Yokoi 1987), feeding ^{179}Ta in small amounts. Neutron captures on ^{179}Ta are dominating over the small β^+ decay back to ^{179}Hf (the terrestrial ^{179}Ta half-life increases by a factor of 2 at TP temperature), producing mainly ^{180}Ta^g, which β^+- and β^- decays into ^{180}Hf and ^{180}W, respectively. This channel yields about 5 per cent of the solar *p*-rich ^{180}W. A minor amount of ^{179}Ta (IR = 0.04) feeds the stable isomer ^{180}Ta^m, contributing 44 per cent of its solar abundance. At the end of the TP, the residual ^{179}Ta abundance β^+ decays to its stable Hf isobar (Fig. 17).

An additional 39 per cent *s*-contribution to ^{180}Ta^m derives from the β^- decay of ^{180}Hf^m. The production of the ^{180}Hf^m isomeric state is weak: only ~1.3 per cent of the total ^{179}Hf MACS feeds ^{180}Hf^m (at 30 keV $\sigma[^{179}\mathrm{Hf}(n,\gamma)^{180}\mathrm{Hf}] = 922 \pm 8$ mbarn; $\sigma[^{179}\mathrm{Hf}(n,\gamma)^{180}\mathrm{Hf}^m] = 11.4 \pm 0.6$ mbarn; KADoNiS). ^{180}Hf^m has short half-life ($t_{1/2} = 5.5$ h), and decays directly to ^{180}Ta^m. This contribution is independent of temperature and is completely determined by the partial cross-section to ^{180}Hf^m.

The final *s*-abundance of ^{180}Ta^m is largely sensitive to temperature and electron density (Takahashi & Yokoi 1987), and needs to be properly evaluated by accounting of the temperature and density gradients over the convective He flashes. Belič et al. (1999, 2002) carried out a photoactivation experiment of ^{180}Ta^m to study the probability for connecting isomer and ground state in ^{180}Ta via thermally induced transitions to higher lying mediating states. Whereas the direct internal decay of the isomer to the ground state is highly forbidden by selection rules, thermal excitations of such mediating states are allowed under stellar conditions. They found that the two states are fully thermalized at $T_8 = 3$: thus, ^{180}Ta^m should be destroyed in the bottom layers of the advanced TPs, where such temperatures are reached. Instead, the fast convective mixing (of the order of a few hours) occurring during TP prevents the destruction of ^{180}Ta^m (see Fig. 17).

Starting from Wisshak et al. (2001, 2004) and Käppeler et al. (2004), our AGB models account for the thermally induced destruction of ^{180}Ta^m obtained by the photoactivation measurement by Belič et al. (1999, 2002), by following the strong half-life variation with temperature and density gradients together with convective mixing at each TP. This method first pointed out that ^{180}Ta^m receives a dominant contribution from the main component, increasing the previous estimate from ~49 per cent (Arlandini et al. 1999) to ~80 per cent (Käppeler et al. 2004; Wisshak et al. 2004). In addition, it provides information on the convective turnover time during He-shell flashes, and underlines that temperature gradient and neutron freeze-out effects are not sufficient to analyse the abundances of such peculiar isotopes correctly.

The main component reproduces about 83 per cent of solar ^{180}Ta^m (see *filled circle* in Fig. 5). This prediction is affected by a number of uncertainties, however. Therefore, the fraction of ~20 per cent, which have to be contributed by other sources, could well be significantly larger.

In order to improve the estimated *s*-contribution to ^{180}Ta^m, we have included the same treatment to the ^{179}Ta β^+-decay and ^{179}Hf β^--decay rates over the full convective zone. The *s*-contribution to ^{180}Ta^m is reduced from ~83 to ~68 per cent (see *filled diamond* in Fig. 5). This value remains strongly sensitive to the uncertain β-decay rate of ^{179}Hf estimated by Goriely (1999) who suggested that the ^{179}Hf β^--decay rate may decrease by a factor of 3, resulting in a strong impact on the contribution to solar ^{180}Ta^m (−30 per cent). The smaller ^{179}Ta β^+-decay uncertainty estimated by Goriely (1999) does not affect ^{180}Ta^m.

As a consequence, AGB stars remain to be the major nucleosynthesis sites for ^{180}Ta^m, but leave a larger fraction for abundance contributions by other processes.

In light of this result, we suggest that an investigation of the ^{179}Hf half-life under stellar conditions would be important in order to assess the contribution to ^{180}Ta^m from AGB stars more reliably.

We examine additional uncertainties associated with the ^{180}Ta^m *s*-prediction. Although the ^{180}Ta^m MACS is rather well known with 6.8 per cent uncertainty (1465 ± 100 mbarn at 30 keV; Wisshak et al. 2004), it is affected by a non-negligible stellar enhancement factor (SEF = 0.87 at 30 keV; KADoNiS). Moreover, the ^{179}Ta MACS is only estimated theoretically with ~30 per cent uncertainty (1334 ± 422 at 30 keV; KADoNiS), producing ~10 per cent variations of the ^{180}Ta^m *s*-abundance.

Finally, the ^{180}Ta^m *s*-prediction decreases by ~12 per cent with increasing the ^{22}Ne(α, n)^{25}Mg rate by a factor of 4 (see Table A1, Supporting Information).

5.4.2 *Updated* s*-contributions to* ^{182}*W and the short-lived* ^{182}*Hf*

The *s*- and *r*-process contributions to solar ^{182}W and ^{182}Hf are mainly regulated by the branch at ^{181}Hf (see Fig. 16). Present AGB predictions marginally produce the short-lived ^{182}Hf ($t_{1/2} = 8.9$ Myr), because the terrestrial half-life of ^{181}Hf is strongly reduced during TPs (from $t_{1/2} = 42.39$ to 1.26 d at $T_8 = 3$; Takahashi & Yokoi 1987) and the *s*-path mainly feeds ^{182}W. We estimate that 65 per cent of solar ^{182}W is synthesized by the main component (see Table A1, Appendix A, Supporting Information), which corresponds to a residual 35 per cent *r*-contribution, in agreement with previous calculations by Wisshak et al. (2006c) and Vockenhuber et al. (2007). This value includes the radiogenic contribution of ^{182}Hf at the end of the TP-AGB phase. Indeed, no β-decay occurs during TPs because the decrease of the ^{182}Hf half-life is not sufficient to compete with neutron captures ($t_{1/2} = 22$ yr at $T_8 = 3$; Takahashi & Yokoi 1987).

Lugaro et al. (2014a) have recently demonstrated that the present AGB contributions to ^{182}Hf and ^{182}W have so far been underestimated. Starting from the experimental work by Bondarenko et al. (2002), who did not find any evidence for the existence of the ^{181}Hf levels responsible for the strong enhancement of the β-decay rate (at 68, 170 and 298 keV), Lugaro et al. (2014a) argued that the terrestrial β-decay rate of ^{181}Hf remains rather unchanged in stellar condition. This favours the neutron capture channel towards ^{182}Hf, which increases the abundance of ^{182}W after the TP-AGB phase. By assuming a constant ^{181}Hf β-decay rate, we find a negligible *r*-contribution to solar ^{182}W, which would be fully produced by AGBs. On the other hand, Lugaro et al. (2014a) estimated a new ^{181}Hf β-decay rate by removing the 68 keV level (see their fig. S2; top panel, blue line). By including this value in our calculations, the *s*-contribution of ^{182}W increases from 65 to 80 per cent, reducing the *r*-component by a factor of 2. The lower limit given by the authors (obtained by removing the three levels; top panel, red line) further increases the solar *s*-abundance of ^{182}W to 86 per cent. The ^{182}W *s*-prediction shows -3 per cent variations within the ^{22}Ne(α, n)^{25}Mg rate uncertainties.

This result is of great relevance to the chronometry of the early Solar system (see Wasserburg et al. 2006 for a review on short-lived isotopes), or in pre-solar stardust grains (Avila et al. 2012).

In addition, it provides another key to explain the apparent anomaly in the *r*-process residuals at $A = 182$, together with the uncertainty associated with the neutron capture cross-sections advanced by Vockenhuber et al. (2007).

5.4.3 *Additional branches mainly sensitive to stellar temperature (and/or electron density)*

Similarly to ^{180}Ta$^{\rm m}$, also the *p*-rich isotope ^{164}Er receives a dominant contribution from the *s*-process owing to the activation of the branch at ^{163}Dy (which becomes unstable in stellar environment).

About 80 per cent of solar ^{164}Er is produced during TPs (*filled circle* in Fig. 5). This value rises to 87 per cent by including an improved treatment of the β-decay rates of nearby unstable isotopes over the convective TPs (see *filled diamond* in Fig. 5). Unfortunately, the *s*-contribution to ^{164}Er cannot be accurately assessed, being largely sensitive to the competition between the β^- and β^+-decay rates of ^{164}Ho, and in particular to the uncertainty of the ^{164}Ho β^--decay rate estimated under stellar conditions (10–20 per cent). We discuss in Appendix B (Supporting Information) the main uncertainties affecting the *s*-contribution to ^{164}Er.

Reifarth et al. (2004) provided a test for the convective mixing time-scale during TPs, by examining the branch at ^{128}I, which regulates the production of the *s*-only pair ^{128,130}Xe. The *s*-predictions of ^{128,130}Xe exhibit a weak dependence on neutron density owing to the short half-lives of ^{127}Te ($t_{1/2} = 9$ h) and ^{128}I ($t_{1/2} = 25$ min), and the competition between ^{128}I β-decay and electron captures may constrain the convective mixing time-scale during the He shell flash. While the β^--decay channel of ^{128}I shows only a weak dependence on temperature, the electron capture rate is strongly temperature-dependent: from $t_{1/2}$(EC) $\sim$ 6 h at $T_8 = 0.5$ up to $\sim$8 d at $T_8 = 3$. By assuming a sufficiently short turnover mixing time-scale, the ^{128}I produced via neutron captures in the hot bottom layers of the TP is promptly brought to the cooler external layers of the convective zone, allowing a partial activation of the EC channel with the result that $\sim$5 to 6 per cent of the *s*-process flow is bypassing ^{128}Xe. The corresponding *s*-predictions for ^{128}Xe and ^{128}Xe are in agreement with the ^{128,130}Xe ratio observed in SiC grains and confirm the results of Reifarth et al. (2004, see Appendix B, Supporting Information). The ^{128,130}Xe *s*-predictions are rather well determined, because the branching is completely regulated by the decay of ^{128}I, so that the influence of uncertain theoretical MACS values of nearby unstable isotopes is negligible at stellar temperatures.

6 SUMMARY AND CONCLUSIONS

Despite a GCE model would provide a more realistic description of the abundances observed in the Solar system, the main component is still a useful tool to investigate the *s*-process nucleosynthesis of nuclei with atomic mass between 90 and 204.

We have studied the major uncertainties affecting the nuclear network. The analysis has been carried out with the most recent neutron capture cross-sections and with updated solar abundance data.

We have examined the impact of the present uncertainties of the two neutron sources operating in AGB stars, the ^{13}C(α, n)^{16}O and ^{22}Ne(α, n)^{25}Mg reactions, focusing on the *s*-only isotopes sensitive to the most important branch points of the main component.

The overall *s*-distribution of isotopes heavier than $A \sim 90$ shows negligible variations (up to $\sim$1 per cent) by changing the ^{13}C(α, n)^{16}O rate by about factor of 2. Only the two neutron-magic nuclei ^{86}Kr and ^{87}Rb are influenced by the ^{13}C(α, n)^{16}O neutron irradiation, because of the marginal activation of the branch at ^{85}Kr. Note, however, that in the AGB models we adopt to reproduce the solar main component ($M = 1.5$ and 3 M$_\odot$ at half solar metallicity), the ^{13}C abundance in the pocket is exhausted radiatively during the interpulse period (only a negligible amount of ^{13}C is engulfed in the subsequent TP). Thus, our AGB models do not experience a partial convective burning of ^{13}C during the first TPs, which could affect the production of a few neutron-rich isotopes (e.g. ^{86}Kr and ^{87}Rb, or ^{96}Zr as well; see Cristallo et al. 2006). The new measurement by La Cognata et al. (2013) suggests that the ^{13}C(α, n)^{16}O rate adopted in our models should be increased by 40 per cent, rather than decreased. In this case, the convective ^{13}C burning during TPs is significantly reduced.

However, beside the undeniable progress made by means of indirect measurements (La Cognata et al. 2013), the existence of a sub-threshold state makes the evaluation of the rate at astrophysical energies still uncertain. A further increase of this rate would likely have marginal consequences on the main component, a substantial reduction may increase the amount of ^{13}C engulfed in the convective pulse and burned at relatively high temperature.

The present uncertainty of ^{22}Ne(α, n)^{25}Mg (e.g. Käppeler et al. 1994; Jaeger et al. 2001; Longland et al. 2012) mainly influences the isotopes close to and within the branchings of the *s*-path.

We have provided new evaluated values of the ^{22}Ne(α, n)^{25}Mg and ^{22}Ne(α, γ)^{26}Mg rates that account for all known and potential resonances as well as all nuclear data available. In the temperature range of AGB stars ($T_8 = 2.5$–3), the recommended ^{22}Ne(α, n)^{25}Mg value is about a factor of 2 lower than that adopted in our models so far, while the recommended ^{22}Ne(α, γ)^{26}Mg rate is essentially unchanged. The recommended rates are in agreement within the errors with the recent values presented in literature (Jaeger et al. 2001; Longland et al. 2012).

However, the ^{22}Ne(α, n)^{25}Mg and ^{22}Ne(α, γ)^{26}Mg rates are mainly based on the knowledge of the 832 keV resonance. As discussed for the ^{13}C(α, n)^{16}O neutron source, the presence of unknown low-energy states, which have been identified in several indirect experiments, makes the ^{22}Ne(α, n)^{25}Mg and ^{22}Ne(α,

$\gamma)^{26}$Mg recommended values uncertain at stellar energy. A direct determination of these reaction rates at temperatures below the present experimental limits will shed light on the actual efficiency of the AGB neutron sources. Because the available low-energy measurements were mainly limited by a significant neutron background, deep underground laboratories are the most promising places to plan future experimental investigations on the two AGB neutron sources (LUNA, DIANA).

For this reason, we have analysed the solar main component within a more cautious range of uncertainty, corresponding to variations by a factor of 4 starting from our recommended ^{22}Ne(α, n)^{25}Mg rate.

Major variations are shown by the *s*-only nuclides close to the branchings, which are most sensitive to neutron density as ^{96}Mo, ^{142}Nd, and ^{170}Yb (due to the branch points at ^{95}Zr, ^{141}Ce, ^{170}Tm), ^{134}Ba and ^{152}Gd (which also depend on the ^{134}Cs and ^{151}Sm half-lives, respectively, both strongly reduced in stellar environments) and ^{176}Lu (affected by the contribution of isomeric mediating states; see Mohr et al. 2009).

In low-mass AGB stars (which are the major contributors to the solar *s*-abundances; Travaglio et al. 2004; Bisterzo et al. 2014), the ^{22}Ne(α, γ)^{26}Mg reaction is not efficiently activated during TPs owing to the rather small temperature reached at the bottom of the advanced convective He flashes. Thus, the competition between ^{22}Ne(α, γ)^{26}Mg and ^{22}Ne(α, n)^{25}Mg reactions is marginal and does not influence the solar *s*-distribution.

A larger impact of the ^{22}Ne(α, γ)^{26}Mg and ^{22}Ne(α, n)^{25}Mg rates is expected from IMS, where the ^{22}Ne(α, n)^{25}Mg is the major neutron source, or from low-metallicity AGB models. The study of these models provides information about the *s*-process nucleosynthesis in, e.g. globular clusters, dwarf galaxies, intrinsic or extrinsic peculiar stars showing *s*-enhancement. To this purpose, we have analysed the rate uncertainties in a 3 $M_\odot$ model at [Fe/H] = −1 and a half-solar metallicity 5 $M_\odot$ model chosen as representative of an extended range of AGB stars.

The status of the (n, γ) stellar cross-sections has been significantly improved in the last decade, with accuracies of less than 5 per cent for a number of isotopes in the mass region $120 < A < 180$. On the other hand, the accuracy of neutron capture and β-decay rates of isotopes that act as important branching points of the *s*-path plays a crucial role in the production of a few *s*-only nuclides. First, because the MACS of unstable isotopes are barely accessible to direct measurements, only theoretical estimates (with large uncertainty) are available in most cases. Secondly, because the stellar β-decay rates are poorly known for branch point nuclei, in particular if they are extremely sensitive to temperature and electron density. Moreover, Rauscher et al. (2011) and Rauscher (2012) highlighted that the (experimentally measured) ground state cross-section may constitute only a minor fraction of the MACS. Thus, the theoretical uncertainties associated with the MACS may be in a few cases underestimated (note that Rauscher et al. 2011 provide upper limits of MACS uncertainties; specific theoretical investigations carried out individually for each nucleus are strongly needed for a few isotopes[8]).

In this study, we have discussed the present major nuclear uncertainties that affect the *s*-only isotopes. We have distinguished the *s*-only nuclei in different classes, according to the type of information that can be deduced from their abundances with respect to the physical conditions in AGB stars: unbranched nuclides (useful to constrain the *s*-distribution), isotopes mainly affected by neutron density, and isotopes strongly sensitive to temperature and electron density (which help to address the characteristics of stellar models). For each class, the specific problems and suggestions for a possible improvement are given. We suggest that an investigation of the β-decay rates as a function of the stellar environment would be important for ^{134}Cs, ^{151}Sm, ^{179}Hf and ^{164}Ho in order to improve the *s*-contributions of ^{134}Ba, ^{152}Gd, ^{180}Ta$^{\rm m}$ and ^{164}Er.

In conclusion, we find that the solar main component may still reproduce the *s*-only isotopes within the present uncertainties.

ACKNOWLEDGEMENTS

We are indebted to I. Dillmann and T. Rauscher for sharing information concerning the nuclear network and the theoretical analysis that significantly improved the present discussion in many ways.

This work has been supported by JINA (Joint Institute for Nuclear Astrophysics, University of Notre Dame, IN) and by KIT (Karlsruhe Institute of Technology, Karlsruhe, Germany).

REFERENCES

Abia C. et al., 2002, ApJ, 579, 817
Anders E., Grevesse N., 1989, Geochim. Cosmochim. Acta, 53, 197
Angulo C. et al., 1999, Nucl. Phys. A, 656, 3
Arcones A., Thielemann F.-K., 2013, J. Phys. G: Nucl. Part. Phys., 40, 013201
Arlandini C., Käppeler F., Wisshak K., Gallino R., Lugaro M., Busso M., Straniero O., 1999, ApJ, 525, 886
Arnett W. D., Thielemann F.-K., 1985, ApJ, 295, 589
Avila A. N. et al., 2012, ApJ, 744, 49
Bao Z. Y., Beer H., Käppeler F., Voss F., Wisshak K., 2000, At. Data Nucl. Data Tables, 76, 70
Beer H., Macklin R. L., 1985, Phys. Rev. C, 32, 738
Belič D. et al., 1999, Phys. Rev. Lett., 83, 5242
Belič D. et al., 2002, Phys. Rev. Lett., 65, 035801
Best J. et al., 2001, Phys. Rev. C, 64, 015801
Bisterzo S., Gallino R., Straniero O., Cristallo S., Käppeler F., 2010, MNRAS, 404, 1529
Bisterzo S., Gallino R., Straniero O., Cristallo S., Käppeler F., 2011, MNRAS, 418, 284
Bisterzo S., Travaglio C., Gallino R., Wiescher M., Käppeler F., 2014, ApJ, 787, 10
Bondarenko V. et al., 2002, Nucl. Phys. A, 709, 3
Bosch F. et al., 1996, Phys. Rev. Lett., 77, 5190
Busso M., Lambert D. L., Beglio L., Gallino R., Raiteri C. M., Smith V. V., 1995, ApJ, 446, 775
Busso M., Gallino R., Wasserburg G. J., 1999, ARA&A, 37, 239
Busso M., Gallino R., Lambert D. L., Travaglio C., Smith V. V., 2001, ApJ, 557, 802
Busso M., Palmerini S., Maiorca E., Trippella O., Magrini L., Randich S., 2012, Proc. XII International Symp. on Nuclei in the Cosmos (NIC XII). Cairns, Australia
Caughlan G. R., Fowler W. A., 1988, At. Data Nucl. Data Tables, 40, 283
Chiaveri E. et al., 2012, EPJ Web Conf., 21, 03001
Chieffi A., Limongi M., 2013, ApJ, 764, 21
Clayton D. D., Rassbach M. E., 1967, ApJ, 148, 69
Clayton D. D., Ward R. A., 1974, ApJ, 193, 397
Cosner K., Iben I. I., Truran J. W., 1980, ApJ, 238, L91
Costantini H., Formicola A., Imbriani G., Junker M., Rolfs C., Strieder F., 2009, Rep. Prog. Phys. 72, 086301

---

[8] Specific cases are ^{134}Cs, ^{151}Sm and ^{154}Eu, ^{164}Ho, ^{179}Hf, ^{185}W, ^{192}Ir, in order to improve the *s*-contributions of ^{134}Ba, $^{152,\,154}$Gd, ^{164}Er, ^{180}Ta$^{\rm m}$, ^{186}Os, ^{192}Pt, as well as ^{160}Dy, ^{164}Er, ^{170}Yb, ^{176}Hf, ^{180}Ta$^{\rm m}$, which are directly influenced.

Cristallo S., Gallino R., Straniero O., Piersanti L., Domínguez I., 2006, Mem. Soc. Astron. Ital., 77, 774

Cristallo S., Straniero O., Gallino R., Piersanti L., Domínguez I., Lederer M. T., 2009, ApJ, 696, 797

Cristallo S., Piersanti L., Gallino R., Straniero O., Käppeler F., Domínguez I., Mohr P., 2010, J. Phys.: Conf. Ser., 202, 012033

Cristallo S. et al., 2011, ApJS, 197, 17

Cyburt R. H. et al., 2010, ApJSS, 189, 240

D'Orazi V., Lugaro M., Campbell S. W., Bragaglia A., Carretta E., Gratton R. G., Lucatello S., D'Antona F., 2013, ApJ, 776, 59

De Smedt K., Van Winckel H., Kamath D., Karakas A. I., Siess L., Goriely S., Wood P., 2014, A&A, 563, 5

deBoer R. J., Wiescher M., Görres J., Longland R., Iliadis C., Rusev G., Tonchev A. P., 2010, Phys. Rev. C, 82, 025802

Denissenkov P. A., Tout C. A., 2003, MNRAS, 340, 722

Denker A. et al., 1995, in Busso M., Raiteri C. M., Gallino R., eds, AIP Conf. Proc. Vol. 327, Nuclei in the Cosmos III, Third International Symposium on Nuclear Astrophysics. Am. Inst. Phys., New York, p. 255

Doherty C. L., Gil-Pons P., Lau H. H. B., Lattanzio J. C., Siess L., 2014, MNRAS, 437, 195

Doll C., Borner H., Jaag S., Käppeler F., 1999, Phys. Rev. C, 59, 492

Domingo-Pardo C. et al., 2007, Phys. Rev. C, 75, 015806

Dracoulis G. D. et al., 2010, Phys. Rev. C, 81, 011301R

Drotleff H. W. et al., 1993, ApJ, 414, 735

Frischknecht U., Hirschi R., Thielemann F.-K., 2012, A&A, 538, L2

Frost C. A., Lattanzio J. C., 1996, ApJ, 473, 383

Fujii K. et al., 2010, Phys. Rev. C, 82, 015804

Gallino R., Arlandini C., Busso M., Lugaro M., Travaglio C., Straniero O., Chieffi A., Limongi M., 1998, ApJ, 497, 388

Giesen U. et al., 1993, Nucl. Phys. A, 561, 95

Gintautas V., Champagne A. E., Kondev F. G., Longland R., 2009, Phys. Rev. C, 80, 015806

Gonzalez G., 2014, MNRAS, 443, L99

Goriely S., 1999, A&A, 342, 881

Goriely S., Siess L., 2004, A&A, 421, L25

Gosselin G., Morel P., Mohr P., 2010, Phys. Rev. C, 81, 055808

Guandalini R., Cristallo S., 2013, A&A, 555, 120

Guo B. et al., 2012, ApJ, 756, 193

Hale G., 1997, Nucl. Phys. A, 621, 177

Hansen C. J., Andersen A. C., Christlieb N., 2014, A&A, 568, 47

Hayakawa T., Shizuma T., Kajino T., Chiba S., Shinohara N., Nakagawa T., Arima T., 2005, ApJ, 628, 533

Heger A., Kolbe E., Haxton W. C., Langanke K., Martinez-Pinedo G., Woosley S. E., 2005, Phys. Lett. B, 606, 258

Heil M., Käppeler F., Uberseder E., Gallino R., Bisterzo S., Pignatari M., 2008a, Phys. Rev. C, 78, 025802

Heil M. et al., 2008b, Phys. Rev. C, 78, 025803

Heil M. et al., 2008c, ApJ, 673, 434

Heil M., Juseviciute A., Käppeler F., Gallino R., Pignatari M., Uberseder E., 2009, PASA, 26, 243

Heil M. et al., 2014, Phys. Rev. C, 90, 5804

Herwig F., 2004, ApJ, 605, 425

Herwig F., 2005, ARA&A, 43, 435

Herwig F., Blöcker T., Schönberner D., El Eid M., 1997, A&A, 324, L81

Herwig F., Langer N., Lugaro M., 2003, ApJ, 593, 1056

Iben I. J., Renzini A., 1983, ARA&A, 21, 271

Ivans I. I., Sneden C., Gallino R., Cowan J. J., Preston G. W., 2005, ApJ, 627, 1450

Jaag S., Käppeler F., 1996, ApJ, 464, 874

Jaeger M., Kunz R., Mayer A., Hammer J. W., Staudt G., Kratz K. L., Pfeiffer B., 2001, Phys. Rev. Lett., 87, 202501

Johnson E. D. et al., 2006, Phys. Rev. Lett., 97, 192701

Jung M. et al., 1992, Phys. Rev. Lett., 69, 2164

Käppeler F., Beer H., Wisshak K., 1989, Rep. Prog. Phys., 52, 945

Käppeler F. et al., 1994, ApJ, 437, 396

Käppeler F. et al., 2004, Phys. Rev. C, 69, 055802

Käppeler F., Gallino R., Bisterzo S., Aoki W., 2011, Rev. Mod. Phys., 83, 157

Karakas A. I., Lattanzio J., 2003, PASA, 20, 279

Karakas A. I., Lattanzio J., 2007, PASA, 24, 103

Karakas A. I., Lattanzio J. C., 2014, PASA, 31, 30

Karakas A. I., Lugaro M. A., Wiescher M., Görres J., Ugalde C., 2006, ApJ, 643, 471

Karakas A. I., García-Hernández D. A., Lugaro M., 2012, ApJ, 751, 8

Kashiv Y., Davis A. M., Cai Z., Lai B., Sutton S. R., Lewis R. S., Gallino R., Clayton R. N., 2006, 37th Annual Lunar and Planetary Science Conference. League City, TX

Kashiv Y., Davis A. M., Gallino R., Cai Z., Lai B., Sutton S. R., Clayton R. N., 2010, ApJ, 713, 212

Keeley P., Kemper K., Khoa D. T., 2003, Nucl. Phys. A, 726, 159

Klay N., Käppeler F., 1988, Phys. Rev. C, 38, 295

Klay N., Käppeler F., Beer H., Schatz G., 1991, Phys. Rev. C, 44, 2839

Koehler P. E., 2002, Phys. Rev. C, 66, 055805

Koehler P. E., Guber K. H., 2013, Phys. Rev. C., 88, 035802

Kubono S. et al., 2003, Phys. Rev. Lett., 90, 062501

La Cognata M. et al., 2013, ApJ, 777, 143

Lambert D. L., Smith V. V., Busso M., Gallino R., Straniero O., 1995, ApJ, 450, 302

Langer N., Heger A. Wellstein S., Herwig F., 1999, A&A, 346, L37

Lederer M. T., Aringer B., 2009, A&A, 494, 403

Lederer C. et al., 2013, Phys. Rev. Lett., 110, 022501

Lederer C. et al., 2014, Phys. Rev. C, 89, 025810

Lemut A. et al., 2011, Phys. Rev. Spec. Top. - Accelerators and Beams, 14, 100101

Limongi M., Straniero O., Chieffi A., 2000, ApJS, 129, 625

Liu N. et al., 2014, ApJ, 786, 66

Lodders K., 2003, ApJ, 591, 1220

Lodders K., Palme H., Gail H.-P., 2009, in Trümper J. E., ed., Landolt-Börnstein - Group VI Astronomy and Astrophysics Numerical Data and Functional Relationships in Science and Technology, 4B: Solar System, 4.4. Springer-Verlag, Berlin, p. 44

Longland R., Iliadis C., Rusev G., Tonchev A. P., Deboer R. J., Görres J., Wiescher M., 2009, Phys. Rev. C, 80, 055803

Longland R., Iliadis C., Karakas A. I., 2012, Phys. Rev. C, 85, 065809

Lugaro M., Karakas A. I., Stancliffe R. J., Rijs C., 2012, ApJ, 747, 2

Lugaro M. et al., 2014a, Science, 345, 650

Lugaro M., Tagliente G., Karakas A. I., Milazzo P. M., Käppeler F., Davis A. M., Savina M. R., 2014b, ApJ, 780, 95

Maiorca E., Magrini L., Busso M., Randich S., Palmerini S., Trippella O., 2012, ApJ, 747, 53

Marganiec J., Dillmann I., Domingo Pardo C., Käppeler F., Walter S., 2010, Phys. Rev. C, 82, 035806

Marrone S. et al., 2006, Phys. Rev. C., 73, 034604

Massimi C., 2014, Proceedings of Science (PoS), Nuclei in the Cosmos - XIII, Debrecen, Hungary, p. 055

Massimi C. et al., 2012, Phys. Rev. C, 85, 044615

Merrill P. W., 1952, Science, 115, 484

Mohr P., 2008, Proceedings of Science (PoS), Nuclei in the Cosmos - X, p. 81

Mohr P. et al., 2004, Phys. Rev. C, 69, 032801

Mohr P., Käppeler F., Gallino R., 2007, Phys. Rev. C., 75, 012802R

Mohr P., Bisterzo S., Gallino R., Käppeler F., Kneissl U., Winckler N., 2009, Phys. Rev. C., 79, 045804

Mosconi M. et al., 2010, Phys. Rev. C, 82, 015802

Mowlavi N., Goriely S., Arnould M., 1998, A&A, 330, 206

Müller S., Kretschmer A., Sonnabend K., Zilges A., Galaviz D., 2006, Phys. Rev. C, 73, 025804

Mutti P., Beer H., Brusegan A., Corvi F., Gallino R., 2005, in Haight R. C., Chadwick M. B., Kawano T., Talou P., eds, AIP Conf. Proc., Vol. 769, International Conference on Nuclear Data for Science and Technology. Am. Inst. Phys., New York, p. 1327

Németh Zs ., Käppeler F., Reffo G., 1992, ApJ, 392, 277

Nomoto K., Kobayashi C., Tominaga N., 2013, ARA&A, 51, 457

Patronis N. et al., 2004, Phys. Rev. C, 69, 025803

Pellegriti M. G. et al., 2008, Phys. Rev. C, 77, 042801

Piersanti L., Cristallo S., Straniero O., 2013, ApJ, 774, 98

Pignatari M. et al., 2013a, ApJS, preprint (arXiv:1307.6961)
Pignatari M. et al., 2013b, ApJ, 762, 31
Ratzel U. et al., 2004, Phys. Rev. C, 70, 065803
Rauscher T., 2012, ApJ, 755, L10
Rauscher T., 2014, AIP Adv., 4, 041012
Rauscher T., Thielemann F.-K., 2000, At. Data Nucl. Data Tables, 75, 1
Rauscher T., Heger A., Hoffman R., Woosley S., 2002, ApJ, 576, 323
Rauscher T., Mohr P., Dillmann I., Plag R., 2011, ApJ, 738, 143
Raut R. et al., 2013, Phys. Rev. Lett., 111, 112501
Rayet M. Arnould M., Hashimoto M., Prantzos N., Nomoto K., 1995, A&A, 298, 517
Reifarth R. et al., 2002, Phys. Rev. C, 66, 064603
Reifarth R. et al., 2003, ApJ, 582, 1251
Reifarth R., Käppeler F., Voss F., Wisshak K., Gallino R., Pignatari M., Straniero O., 2004, ApJ., 614, 363
Reifarth R., Dababneh S., Heil M., Käppeler F., Plag R., Sonnabend K., Uberseder E., 2012, Phys. Rev. C, 85, 035802
Reifarth R., Lederer C., Käppeler F., 2014, J. Phys. G: Nucl. Part. Phys., 41, 053101
Reimers D., 1977, A&A, 61, 217
Romano D., Karakas A. I., Tosi M., Matteucci F., 2010, A&A, 522, 32
Shizuma T. et al., 2005, Phys. Rev. C, 72, 025808
Siess L., Goriely S., Langer N., 2004, A&A, 415, 1089
Smith V. V., Lambert D. L., 1990, ApJS, 72, 387
Sneden C., Cowan J. J., Gallino R., 2008, ARA&A, 46, 241
Sonnabend K. et al., 2003, ApJ, 583, 506
Straniero O., Gallino R., Busso M., Chieffi A., Raiteri C. M., Limongi M., Salaris M., 1995, ApJ, 440, L85
Straniero O., Chieffi A., Limongi M., Busso M., Gallino R., Arlandini C., 1997, ApJ, 478, 332
Straniero O., Domínguez I., Cristallo S., Gallino R., 2003, PASA, 20, 389
Straniero O., Gallino R., Cristallo S., 2006, Nucl. Phys. A, 777, 311
Straniero O., Cristallo S., Piersanti L., 2014, ApJ, 785, 77
Tagliente G. et al., 2010, Phys. Rev. C, 81, 055801
Tagliente G. et al., 2011a, Phys. Rev. C, 84, 015801
Tagliente G. et al., 2011b, Phys. Rev. C, 84, 055802
Tagliente G. et al., 2013, Phys. Rev. C, 87, 014622
Takahashi K., Yokoi K., 1987, At. Data Nucl. Data Tables, 36, 375
Tolstoy E., Hill V., Tosi M., 2009, ARA&A, 47, 371
Toukan K., Käppeler F., 1990, ApJ, 348, 357.
Travaglio C., Gallino R., Busso M., Gratton R., 2001, ApJ, 549, 346
Travaglio C., Gallino R., Arnone E., Cowan J., Jordan F., Sneden C., 2004, ApJ, 601, 864
Travaglio C., Gallino R., Rauscher T., Roepke F. K., Hillebrandt W., 2015, ApJ, 799, 54
Truran J. W., Iben I., Jr, 1977, ApJ, 216, 797
Ugalde C. et al., 2007, Phys. Rev. C, 76, 025802
Ulrich R. K., 1973, in Schramm D. N., Arnett D. W., eds, Explosive Nucleosynthesis. University of Texas Press, Austin, TX, p. 139
Utsunomiya H. et al., 2013, Phys. Rev. C, 88, 015805
Van Eck S., Goriely S., Jorissen A., Plez B., 2001, Nature, 412, L23
van Raai M. A., Lugaro M., Karakas A. I., García-Hernández D. A., Yong D., 2012, A&A, 540, 44
Ventura P., DAntona F., 2005, A&A, 439, 1075
Ventura P., Marigo P., 2010, MNRAS, 408, 2476
Vockenhuber C. et al., 2007, Phys. Rev. C, 75, 015804
Wallerstein G., Dominy J. F., 1988, ApJ, 330, 937
Wallerstein G., Iben I. J., Parker P. et al., 1997, Rev. Mod. Phys., 69, 4
Ward R. A., 1977, ApJ, 216, 540
Wasserburg G. J., Busso M., Gallino R., Nollett K. M., 2006, Nucl. Phys. A, 777, 5
Wiescher M., Käppeler F., Langanke K., 2012, ARA&A, 50, 165
Winters R. R., Macklin R. L., 1987, ApJ, 313, 808
Wisshak K. et al., 2001, Phys. Rev. C, 66, 025801
Wisshak K., Voss F., Arlandini C., Käppeler F., Heil M., Reifarth R., Krticka M., Becvar F., 2004, Phys. Rev. C, 69, 055801
Wisshak K., Voss F., Käppeler F., Krticka M., Raman S., Mengoni A., Gallino R., 2006a, Phys. Rev. C, 73, 015802
Wisshak K., Voss F., Käppeler F., Kazakov L., 2006b, Phys. Rev. C, 73, 015807
Wisshak K., Voss F., Käppeler F., Kazakov L., Becvar F., Krticka M., Gallino R., Pignatari M., 2006c, Phys. Rev. C, 73, 045807
Xu Y., Goriely S., Jorissen A., Chen G. L., Arnould M., 2013a, A&A, 549, A106
Xu Y., Takahashi K., Goriely S., Arnould M., Ohta M., Utsunomiya H., 2013b, Nucl. Phys. A, 918, 61
Žugec P. et al., 2014, Phys. Rev. C, 89, 014605

SUPPORTING INFORMATION

Additional Supporting Information may be found in the online version of this article:

Appendix A. The results for the updated main component obtained in the analysis described in Section 2 are listed in Table A1 for the isotopes with A > 70. We also report the effects of the tests discussed in Section 4.1.

Appendix B. This appendix completes the information about the most important branches of the main component discussed in the paper. Following the classification given in Section 5, we analyse here the additional branchings of each category, which are only briefly outlined in the text.

Appendix C. In this appendix, we have analysed the uncertainties of the neutron sources in a $3\,\mathrm{M}_{\odot}$ model at [Fe/H] = −1 and a half-solar metallicity $5\,\mathrm{M}_{\odot}$ model chosen as representative of an extended range of AGB stars.
(http://mnras.oxfordjournals.org/lookup/suppl/doi:10.1093/mnras/stv271/-/DC1).

This paper has been typeset from a TEX/LATEX file prepared by the author.